Article

Cancer Cell

Hippo Signaling Suppresses Cell Ploidy and Tumorigenesis through Skp2

Graphical Abstract

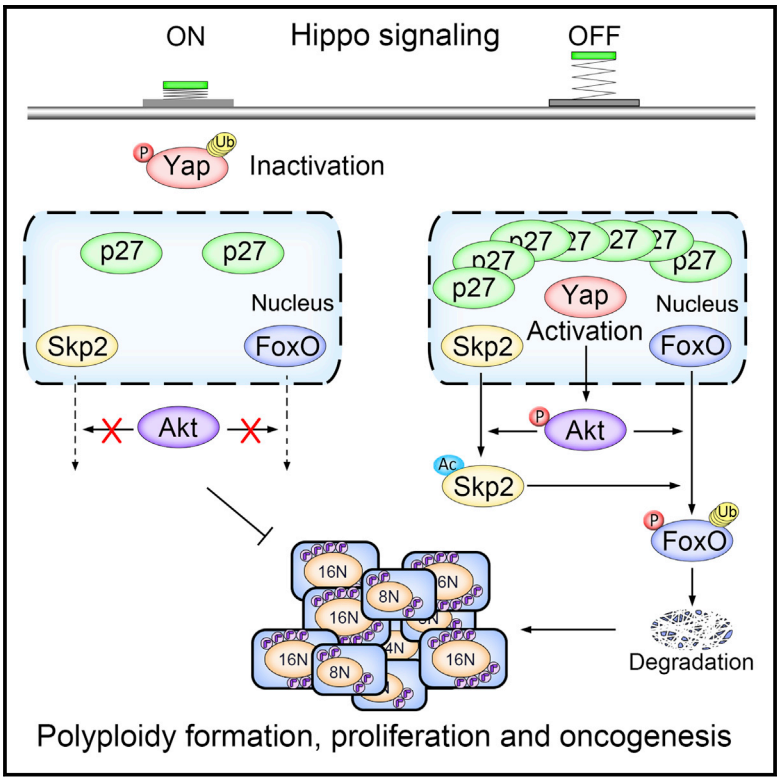

Authors

Shihao Zhang, Qinghua Chen, Qingxu Liu, ..., Daming Gao, Lanfen Chen, Dawang Zhou

Correspondence

chenlanfen@xmu.edu.cn (L.C.), dwzhou@xmu.edu.cn (D.Z.)

In Brief

Zhang et al. show that Yap promotes polyploidy and polyploid cell growth via Akt signaling and p300-mediated acetylation of Skp2, which causes Skp2 cytosolic retention and differential regulation of p27 and FoxO1/3 stabilities. Dysregulated Hippo-Yap-Skp2 axis is associated with human hepatocellular carcinomas.

Highlights

- Yap activation promotes cell polyploidy
- Yap regulates cell polyploidy via Akt-Skp2-p27/FoxO axis
- Yap regulates Skp2 acetylation, cellular relocation, and activation
- Yap differentially regulates FoxO1/3 and p27 stability via Skp2

Zhang et al., 2017, Cancer Cell *31*, 669–684
May 8, 2017
http://dx.doi.org/10.1016/j.ccell.2017.04.004

Cancer Cell
Article

Hippo Signaling Suppresses Cell Ploidy and Tumorigenesis through Skp2

Shihao Zhang,[1,10] Qinghua Chen,[1,10] Qingxu Liu,[1,10] Yuxi Li,[1] Xiufeng Sun,[1] Lixin Hong,[1] Suyuan Ji,[1] Chengyan Liu,[1] Jing Geng,[1] Weiji Zhang,[1] Zhonglei Lu,[4] Zhen-Yu Yin,[2] Yuanyuan Zeng,[3] Kwang-Huei Lin,[5] Qiao Wu,[1] Qiyuan Li,[3] Keiko Nakayama,[6] Keiich I. Nakayama,[7] Xianming Deng,[1] Randy L. Johnson,[8] Liang Zhu,[4] Daming Gao,[9] Lanfen Chen,[1,*] and Dawang Zhou[1,11,*]

[1]State Key Laboratory of Cellular Stress Biology, Innovation Center for Cell Signaling Network, School of Life Sciences, Xiamen University, Xiamen, Fujian 361102, China
[2]Department of Hepatobiliary Surgery, Zhongshan Hospital of Xiamen University, Xiamen, Fujian 361004, China
[3]Department of Translational Medicine, Medical College of Xiamen University, Xiamen, Fujian 361102, China
[4]Department of Developmental and Molecular Biology, Albert Einstein College of Medicine, Bronx, NY 10461, USA
[5]Department of Biochemistry, College of Medicine, Chang Gung University, Liver Research Center, Chang Gung Memorial Hospital, TaoYuan 333, Taiwan, ROC
[6]Division of Cell Proliferation, United Centers for Advanced Research and Translational Medicine, Tohoku University Graduate School of Medicine, Sendai 980-8575, Japan
[7]Division of Cell Regulation Systems, Medical Institute of Bioregulation, Kyushu University, Fukuoka 812-8582, Japan
[8]Department of Biochemistry and Molecular Biology, University of Texas, M.D. Anderson Cancer Center, Houston, TX 77030, USA
[9]Key Laboratory of System Biology, CAS Center for Excellence in Molecular Cell Science, Innovation Center for Cell Signaling Network, Institute of Biochemistry and Cell Biology, Shanghai Institutes for Biological Sciences, Chinese Academy of Sciences, Shanghai 200031, China
[10]These authors contributed equally
[11]Lead Contact
*Correspondence: chenlanfen@xmu.edu.cn (L.C.), dwzhou@xmu.edu.cn (D.Z.)
http://dx.doi.org/10.1016/j.ccell.2017.04.004

SUMMARY

Polyploidy can lead to aneuploidy and tumorigenesis. Here, we report that the Hippo pathway effector Yap promotes the diploid-polyploid conversion and polyploid cell growth through the Akt-Skp2 axis. Yap strongly induces the acetyltransferase p300-mediated acetylation of the E3 ligase Skp2 via Akt signaling. Acetylated Skp2 is exclusively localized to the cytosol, which causes hyper-accumulation of the cyclin-dependent kinase inhibitor p27, leading to mitotic arrest and subsequently cell polyploidy. In addition, the pro-apoptotic factors FoxO1/3 are overly degraded by acetylated Skp2, resulting in polyploid cell division, genomic instability, and oncogenesis. Importantly, the depletion or inactivation of Akt or Skp2 abrogated Hippo signal deficiency-induced liver tumorigenesis, indicating their epistatic interaction. Thus, we conclude that Hippo-Yap signaling suppresses cell polyploidy and oncogenesis through Skp2.

INTRODUCTION

Polyploidy is a state in which cells possess more than two sets of homologous chromosomes. Although it is less frequently found in animals, some tissues, including the liver, have a high percentage of polyploid cells. Polyploid hepatocytes undergo ploidy reversal to specifically generate unique hepatocytes with different mixtures of chromosomes (Duncan, 2013; Gentric and Desdouets, 2014; Pandit et al., 2013). This genetic diversity may be an adaptive mechanism, serving as a means for the

Significance

p53 is required for the induction of cell senescence to limit the proliferation of polyploid cells. We found that Hippo signal deficiency or Yap activation in mouse livers result in polyploid formation and polyploid cell growth. The combined loss of Hippo signals and p53 lead to greatly increased polyploidy and result in a higher incidence and earlier onset of liver tumors. We revealed that Yap induces cell polyploidy through the Skp2-mediated ubiquitin-proteasome pathway. Importantly, the deregulation of the Hippo-Yap-Skp2 axis is found in a substantial fraction of human hepatocellular carcinomas. Thus, Hippo-Yap signaling acts as an alternative polyploid checkpoint, together with p53, to synergistically restrain polyploid cell division, thus limiting the risk of genomic instability, aneuploidy, and tumorigenesis.

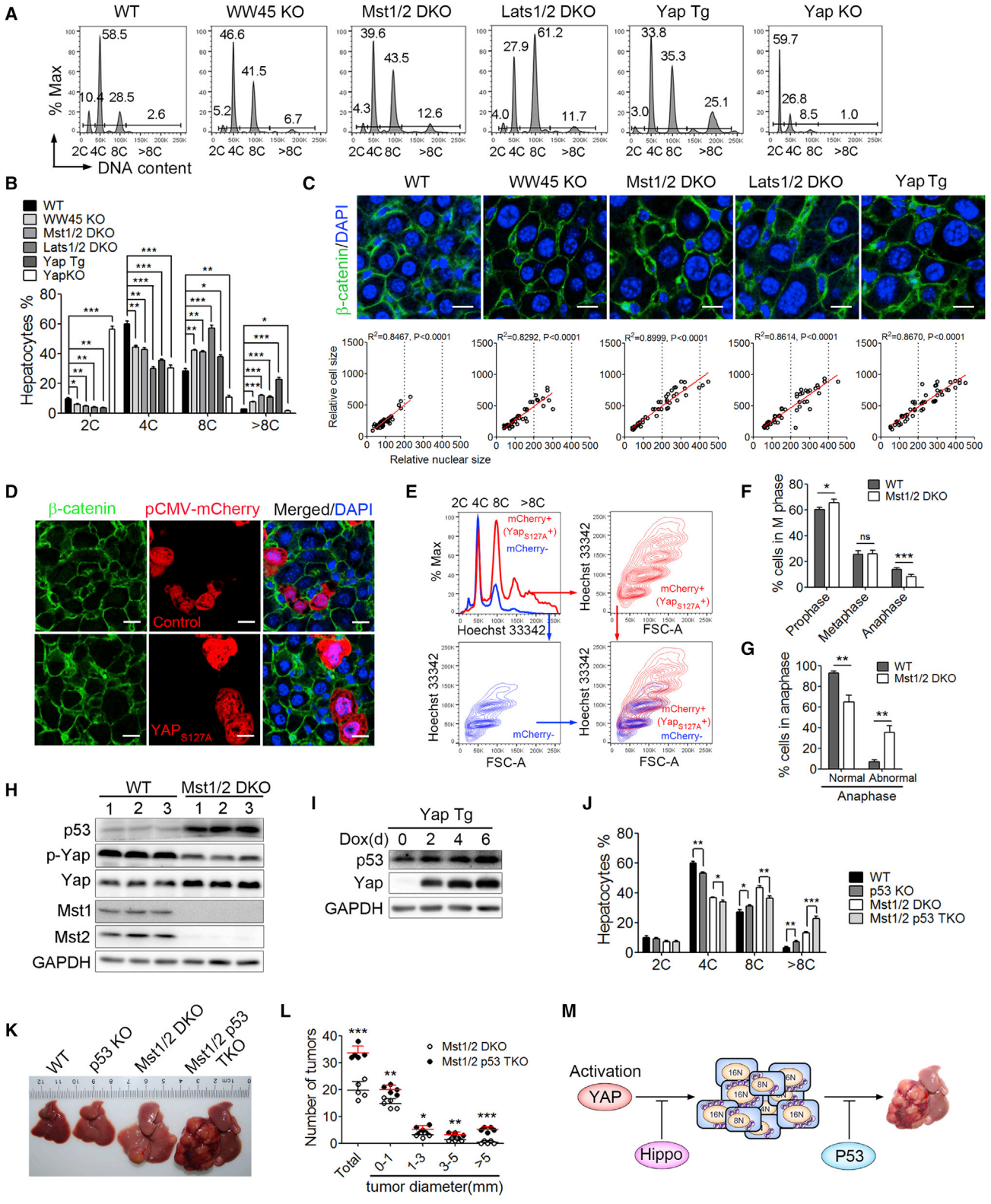

Figure 1. Yap Activation Increases Hepatocyte Polyploidy and Synergizes with p53 Inactivation to Enhance Liver Tumorigenesis

(A and B) Fluorescence-activated cell sorting (FACS) analysis (A) and the DNA content quantification (B) of polyploid hepatocytes from wild-type (WT), *WW45*$^{f/f}$*Alb*-Cre (WW45 KO), *Mst1*$^{f/f}$*Mst2*$^{f/f}$*Alb*-Cre (Mst1/2 DKO), *Lats1*$^{f/f}$*Lats2*$^{f/f}$*Alb*-Cre (Lats1/2 DKO), Yap (S127A) transgenic (Yap Tg), and *Yap*$^{f/f}$*Alb*-Cre (Yap KO) mice (n = 3). 2C, 4C, 8C, and >8C DNA content, corresponding to diploid, tetraploid, octaploid, and higher polyploid hepatocytes, respectively.

(legend continued on next page)

selection of hepatocytes most resistant to xenobiotic or nutritional injury. Gene redundancy shields polyploids from the deleterious effects of mutations (Duncan et al., 2009, 2010). However, polyploid cells precede aneuploid cells that give rise to increased genomic instability and tumor progression (Davoli and de Lange, 2011; Ganem and Pellman, 2007; Gordon et al., 2012). Consistently, two-thirds partial hepatectomy (PH)-induced liver regeneration results in increased cell polyploidy and causes the normally quiescent polyploid hepatocytes to undergo cell-cycle re-entry and division, accelerating the ability of oncogenes to induce hepatocellular carcinoma (HCC) (Beer et al., 2004). Polyploid cells are normally arrested in the G1 phase of the cell cycle, thus preventing genomic instability, aneuploidy, and tumorigenesis. Thus, it is of particular interest to determine the mechanisms regulating polyploid formation and polyploid cell division.

Cell polyploidy can result from cell fusion or abnormal cell division, including endoreduplication, mitotic slippage and cytokinesis failure (Pandit et al., 2013). Cytokinesis failure and mitotic slippage events have a pivotal role in establishing hepatocyte polyploidy (Celton-Morizur et al., 2009; Hsu et al., 2016; Pandit et al., 2012). Skp2 is a major cytokinetic regulator and an F box protein that targets p27 for ubiquitination and subsequent degradation to promote cell-cycle progression (Carrano et al., 1999; Nakayama et al., 2000, 2004). Skp2-null mice develop a phenotype of polyploidy and centrosome amplification in the liver (Kossatz et al., 2004; Nakayama et al., 2004; Serres et al., 2012). Elevated levels of p27 in the S and G2/M phases upon the depletion of Skp2 cause cytokinesis failure and mitotic slippage events. These phenotypes are completely rescued by the concomitant deletion of p27 (Nakayama et al., 2004). Recent studies revealed that Skp2 stability, sub-cellular localization, and activity are regulated by its phosphorylation and acetylation (Chan et al., 2012; Gao et al., 2009; Inuzuka et al., 2012; Lin et al., 2009). Skp2 expression is highly upregulated in a variety of human cancers (Calvisi et al., 2009; Lee et al., 2015; Lin et al., 2010; Wang et al., 2010; Zhao et al., 2013). These results indicate that certain signaling may be required for the regulation of Skp2 function in controlling cell polyploidy.

The Hippo signaling pathway is a critical regulator of stem cell self-renewal, tissue regeneration, and organ size (Johnson and Halder, 2014; Pan, 2010; Yu et al., 2015). Central to this pathway is a kinase cascade formed by mammalian sterile20 kinases Mst1 and Mst2 (Mst1/2), a scaffolding protein Salvador/WW45 (Sav), an NDR family kinases large tumor suppressor 1 (Lats1) and Lats2, and an adaptor protein Mob1. Mst1/2 phosphorylates and activates Lats1/2-Mob1, which then phosphorylates the yes-associated protein (Yap) or WW domain-containing transcription regulator protein 1 (Taz). Phospho-Yap/Taz is either degraded or sequestered in the cytoplasm by 14-3-3 protein. When the Hippo pathway is inactivated, Yap/Taz translocates to the nucleus and forms a functional hybrid transcriptional factor with TEA domain family members to turn on pro-proliferative and pro-survival genes, enabling cell proliferation. The Hippo pathway also mediates crosstalk with other signaling pathways including the phosphoinositol-3-kinase (PI3K)-Akt pathway (Dupont et al., 2011; Heallen et al., 2011; Tumaneng et al., 2012; Yu et al., 2012). Genetic defects in this pathway in mice lead to tissue overgrowth and cancer development in multiple organs (Camargo et al., 2007; Dong et al., 2007; Zhou et al., 2009). A recent study showed that Hippo signaling is highly activated in polyploid cells (Ganem et al., 2014). p53 is normally required for the induction of cellular senescence to limit polyploid cell growth (Davoli et al., 2010; Fujiwara et al., 2005; Kurinna et al., 2013). Lats2 kinase of the Hippo signaling pathway was reported to stabilize p53 by inhibiting murine double minute 2 (Mdm2) (Aylon et al., 2006; Iida et al., 2004), which resulted in tetraploid cell-cycle arrest. Thus, polyploidy status might trigger Lats2 kinase to activate p53 to prevent polyploidy cell proliferation (Ganem et al., 2014). Interestingly, Yap overexpression dramatically increases hepatocyte polyploidy, suggesting that Yap is a downstream effector of Lats2 kinase in ploidy regulation (Ganem et al., 2014). Recent studies have shown that Yap is phosphorylated by cyclin-dependent kinase 1 (CDK1) and that this mitotic phosphorylation of Yap is required for the activation of the spindle checkpoint in immortalized epithelial cells (Yang et al., 2013, 2015). However, the mechanism by which Yap determines cell ploidy and chromosomal stability remains unclear. Genetic evidence in animals supporting the central role of Hippo signaling in polyploidy formation and subsequent neoplastic transformation is still largely lacking.

RESULTS

Loss of Hippo Signaling Promotes Hepatocyte Polyploidy

Hepatocytes are either mononucleated or binucleated, and each nucleus is diploid, tetraploid, octaploid, or higher, which

(C) Hepatocytes in liver sections from the indicated genotypes were labeled with DAPI and an antibody against β-catenin. The areas of the cell (cell size) and the DAPI-positive compartment (nucleus) were imaged with a Zeiss LSM 780 (upper panel) and quantified using ImageJ software (lower panel). Scale bars, 20 μm.
(D and E) The correlation of hepatocyte size and ploidy status from WT mice after the hydrodynamic delivery of pCMV-mCherry control or pCMV-mCherry-Yap_{S127A} was assessed by immunofluorescent staining (D) and FACS (E) approaches. Scale bars, 20 μm.
(F and G) The quantification of the percentage of cells at the different mitotic phases (F) and the percentage of abnormal anaphase cells (G) according H&E and immunohistochemistry (IHC) staining for pHH3 in liver sections.
(H) Immunoblot analysis of p53, phosphorylated (p-) Yap, Yap, Mst1, Mst2, and GAPDH in WT or Mst1/2 DKO liver tissues.
(I) Immunoblot analysis of p53, Yap, and GAPDH in WT or Yap Tg liver tissues.
(J) The DNA content quantification of polyploid hepatocytes from WT, Mst1/2 DKO, p53KO, or Mst1/2 p53 TKO mice using FACS analysis (n = 3).
(K) A representative liver picture and the liver-to-body weight ratios (n = 5) of 2-month-old WT, Mst1/2 DKO, p53KO, or Mst1/2 p53 TKO mice.
(K and L) A representative liver picture (K) and the quantification of the size and number of liver tumors (n = 5) (L) of 4.5-month-old WT, Mst1/2 DKO, p53KO, or Mst1/2 p53 TKO mice.
(M) A proposed working model for Hippo signaling decreases hepatocyte polyploidy and synergizes with p53 to inhibit liver tumorigenesis.
Data were assessed by Student's t test and represented as mean ± SD. ns, not significant, *$p < 0.05$, **$p < 0.01$, ***$p < 0.001$ compared between indicated groups. See also Figure S1.

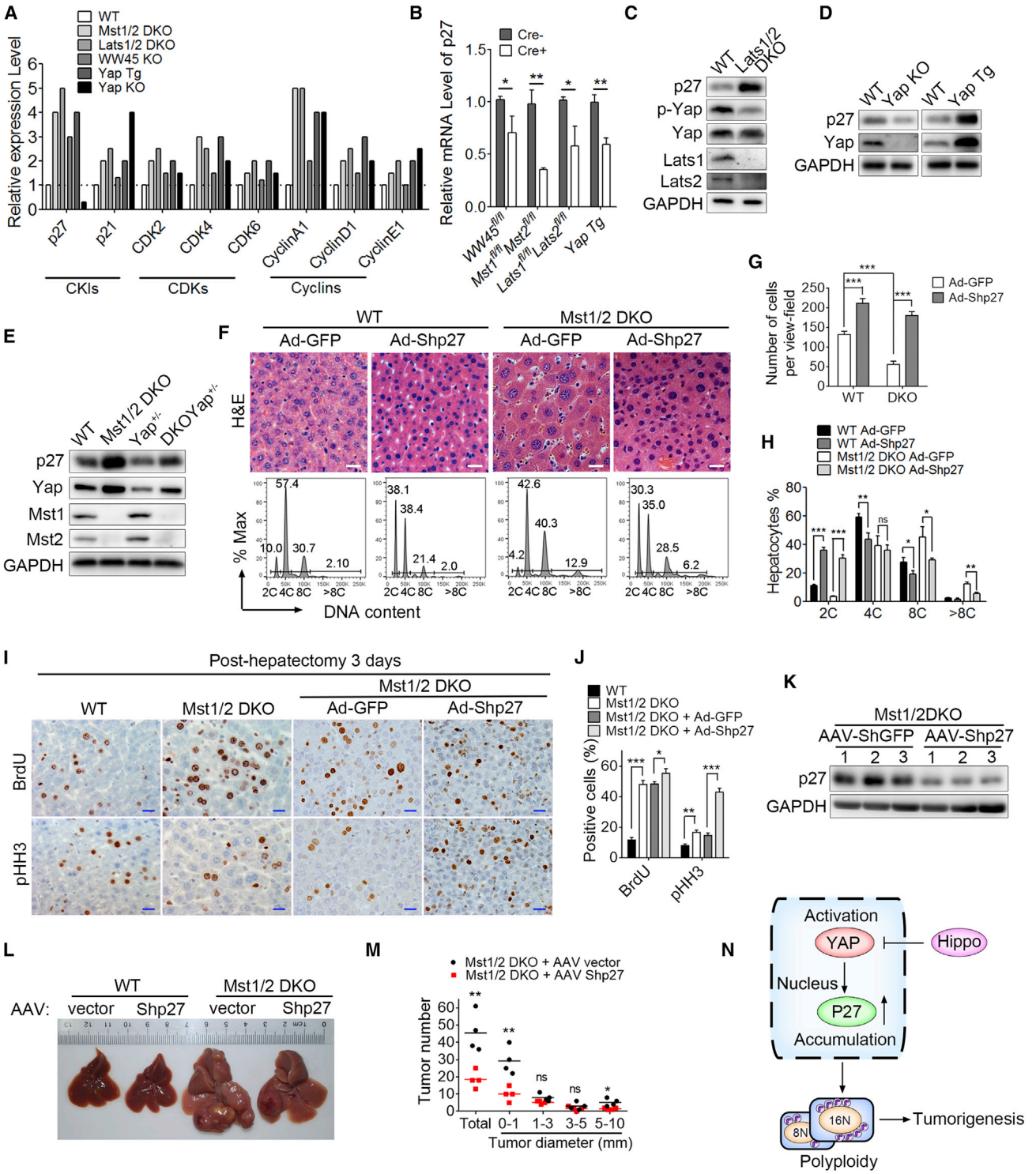

Figure 2. Loss of Hippo Signaling Resulted in the Accumulation of p27 Leading to Polyploidy

(A) The quantification of the relative protein expression levels of cell-cycle-related proteins p27, p21, CDK2, CDK4, CDK6, Cyclin A1, Cyclin D1, and Cyclin E1 in livers from the indicated mouse strains with a liver-specific mutation of the Hippo signaling components.

(B) qPCR analysis of the *p27* mRNA expression in hepatocytes from the indicated liver-specific mutant mice.

(C) Immunoblot analysis of p27, p-Yap, Yap, Lats1, Lats2, and GAPDH in WT or Lats1/2 DKO MEFs.

(D) Immunoblot analysis of p27, Yap, and GAPDH in WT, Yap Tg, or Yap KO control liver tissues.

(E) Immunoblot analysis of p27, Yap, Mst1, Mst2, and GAPDH in WT, Mst1/2 DKO, $Yap^{+/fl}$*Alb*-Cre ($YAP^{+/-}$), or $Mst1^{f/f}Mst2^{f/f}$ $Yap^{+/fl}$*Alb*-Cre (DKO $Yap^{+/-}$) liver tissues.

(legend continued on next page)

makes the liver a valuable organ in which to study cell ploidy regulation. To characterize the function of Hippo signaling on hepatocyte ploidy, we determined the hepatocyte ploidy and nuclear size in liver tissues isolated from various mouse strains with a liver-specific mutation for Hippo signaling components. Compared with wild-type (WT) mice, hepatocytes in the livers of *WW45*$^{f/f}$*Alb*-Cre (WW45 knockout [KO]), *Mst1*$^{f/f}$*Mst2*$^{f/f}$*Alb*-Cre (Mst1/2 double knockout [DKO]), *Lats1*$^{f/f}$*Lats2*$^{f/f}$*Alb*-Cre (Lats1/2 DKO), or doxycycline-inducible active *Yap (S127A)* transgenic (Yap Tg) mice exhibited markedly enlarged nuclear size and increased cell polyploidy, whereas *Yap*$^{f/f}$*Alb*-Cre (Yap KO) animals showed smaller nuclear size and reduced cell polyploidy in the liver (Figures 1A, 1B, S1A, and S1B). In addition, we found that cells of different genotypes with larger nuclei have larger cell sizes (Figure 1C). Furthermore, immunofluorescent staining and flow cytometric analysis clearly showed that Yap transgenic hepatocytes had an increased DNA content and greater cell size (Figures 1D and 1E). These results demonstrated that Hippo signaling plays a critical role in ploidy regulation.

We also found that the loss of Mst1/2 or the overexpression of Yap-induced supernumerary centrosomes and abnormal mitotic spindle formation in dividing hepatocytes (Figures S1C and S1D). In addition, during the regeneration process after PH, more dividing cells at prophase and metaphase were found in Mst1/2 DKO livers than in WT livers (Figures 1F and S1E). Furthermore, fewer cells but with a higher incidence of abnormal anaphase were found in Mst1/2 DKO livers, indicating that cytokinesis failure occurs in Mst1/2 DKO livers (Figure 1G). These data demonstrated that Hippo signaling is important for ensuring accurate centrosome duplication and chromosome segregation to maintain genome stability.

p53 is normally required to induce G1 arrest and cellular senescence in response to tetraploidy or missegregated chromosomes. Lats2 kinase of the Hippo signaling pathway was previously reported to activate and stabilize p53 (Aylon et al., 2006). Surprisingly, we found that the p53 protein levels were dramatically increased in the livers of WW45KO, Mst1/2 DKO, Lats1/2 DKO, and Yap Tg mice compared with those in WT livers (Figures 1H, 1I, S1F, and S1G). We speculated that the highly increased p53 protein levels might be the result of a potent negative feedback loop in response to increased cell polyploidy upon the disruption of Hippo signals. Indeed, the loss of p53 in Mst1/2 DKO (Mst1/2 p53 TKO) mice led to a larger nuclei size and higher polyploidy numbers than those in their Mst1/2 DKO littermates (Figures 1J, S1H, and S1I). Mst1/2 p53 TKO mice also exhibited increased ratios of liver/body weight and accelerated liver tumor formation compared with WT, p53 KO, or Mst1/2 DKO mice (Figures 1K, 1L, and S1J). Taken together, these results indicated that Yap activation increases hepatocyte polyploidy and synergizes with p53 inactivation to enhance liver tumorigenesis (Figure 1M).

Hippo Signal Deficiency Induces Polyploidy via p27

Polyploidy may occur due to cell fusion or abnormal cell division. To identify the potential cell-cycle regulators that induce hepatocyte polyploidy from various mouse strains with liver-specific mutations of the Hippo signaling pathway, we analyzed the protein expression profile of cell-cycle-related proteins, i.e., CKIs (p27 and p21), CDKs (CDK2, CDK4, and CDK6), and cyclins (Cyclin A1, Cyclin D1, and Cyclin E1). We found that only the expression level of p27 was consistently increased in primary hepatocytes from WW45 KO, Mst1/2 DKO, Lats1/2 DKO, and Yap(S127A) Tg mice, but it was decreased in hepatocytes from Yap KO animals (Figures 2A, S2A, and S2B), indicating that p27 might be a direct target downstream of the Hippo signaling pathway. Interestingly, unlike its protein levels, the p27 mRNA level was reduced in Hippo signaling-deficient livers suggesting that the Hippo signaling might regulate the protein stability of p27 (Figure 2B). The positive correlation of p27 levels with Yap activity was further confirmed in primary mouse embryonic fibroblasts (MEFs) isolated from WT, Lats1/2 DKO, Yap(S127A) Tg, or Yap KO mice (Figures 2C–2E), and one *Yap* allele deletion in Mst1/2 DKO liver (Mst1/2 DKO Yap$^{+/-}$) was sufficient to reduce the level of the p27 protein to the level in normal WT hepatocytes (Figures 2E and S2C). These data indicated that Hippo signaling controls the protein level of p27.

Previous studies showed that elevated p27 could cause a failure to enter mitosis and thereby induce polyploidy (Kossatz et al., 2004; Nakayama et al., 2004). We next sought to determine whether the p27 hyper-accumulation is responsible for increased polyploidy in hepatocytes with a Hippo signaling deficiency. Indeed, the ablation of p27 using adenoviral short hairpin RNA (shRNA) (Ad-Shp27) (Figures S2D and S2E) in Hippo signaling-deficient livers or MEF cells resulted in decreased hepatocyte polyploidy and smaller nuclear size (Figures 2F–2H, S2F, and S2G). To determine whether the hyper-accumulation of p27 results in a failure to enter mitosis, we assessed the DNA synthesis rate and mitosis events in Mst1/2-deficient hepatocytes after a PH. Compared with the WT liver, the Mst1/2 DKO liver had a dramatically higher number (approximately 4-fold) of bromodeoxyuridine (BrdU)-positive (DNA synthesis phase) hepatocytes, but a moderately higher level (approximately 2-fold) of phospho-histone H3 (pHH3)-positive (mitosis phase) hepatocytes, indicating that a high fraction of polyploid cells in Mst1/2 DKO liver were arrested in mitosis, whereas the knockdown of

(F–H) H&E staining of liver sections (F, upper panel) and the quantification of cell number per view field (G) or the DNA content quantification (F, lower panel, and H) of polyploid hepatocytes by FACS from WT or Mst1/2 DKO mice infected with either adenovirus expressing a GFP control vector (Ad-GFP) or p27-knockdown shRNA (Ad-Shp27) as indicated (n = 3). Scale bars, 20 μm.

(I and J) IHC staining of BrdU or pHH3 in the liver sections from WT, Mst1/2 DKO, or Mst1/2 DKO mice infected with either Ad-GFP or Ad-Shp27 as indicated after partial hepatectomy (I). The bar graph shows the quantifications of BrdU- or pHH3-positive cells in the livers (n = 3) (J). Scale bars, 20 μm.

(K) Immunoblot analysis of the p27 levels in the livers from Mst1/2 DKO mice infected with adeno-associated virus (AAV) expressing control GFP or p27 shRNA.

(L and M) A representative liver picture (L) and the quantification of the size and number of liver tumors in 4.5-month-old Mst1/2 DKO mice (n = 4) infected with AAV-GFP or AAV-Shp27 (M).

(N) A proposed working model for Yap activation promoting nuclear accumulation of p27 resulted in increased polyploidy and tumor formation.

Data were assessed by Student's t test and represented as mean ± SD. ns, not significant, *p < 0.05, **p < 0.01, ***p < 0.001 compared between the indicated groups. See also Figure S2.

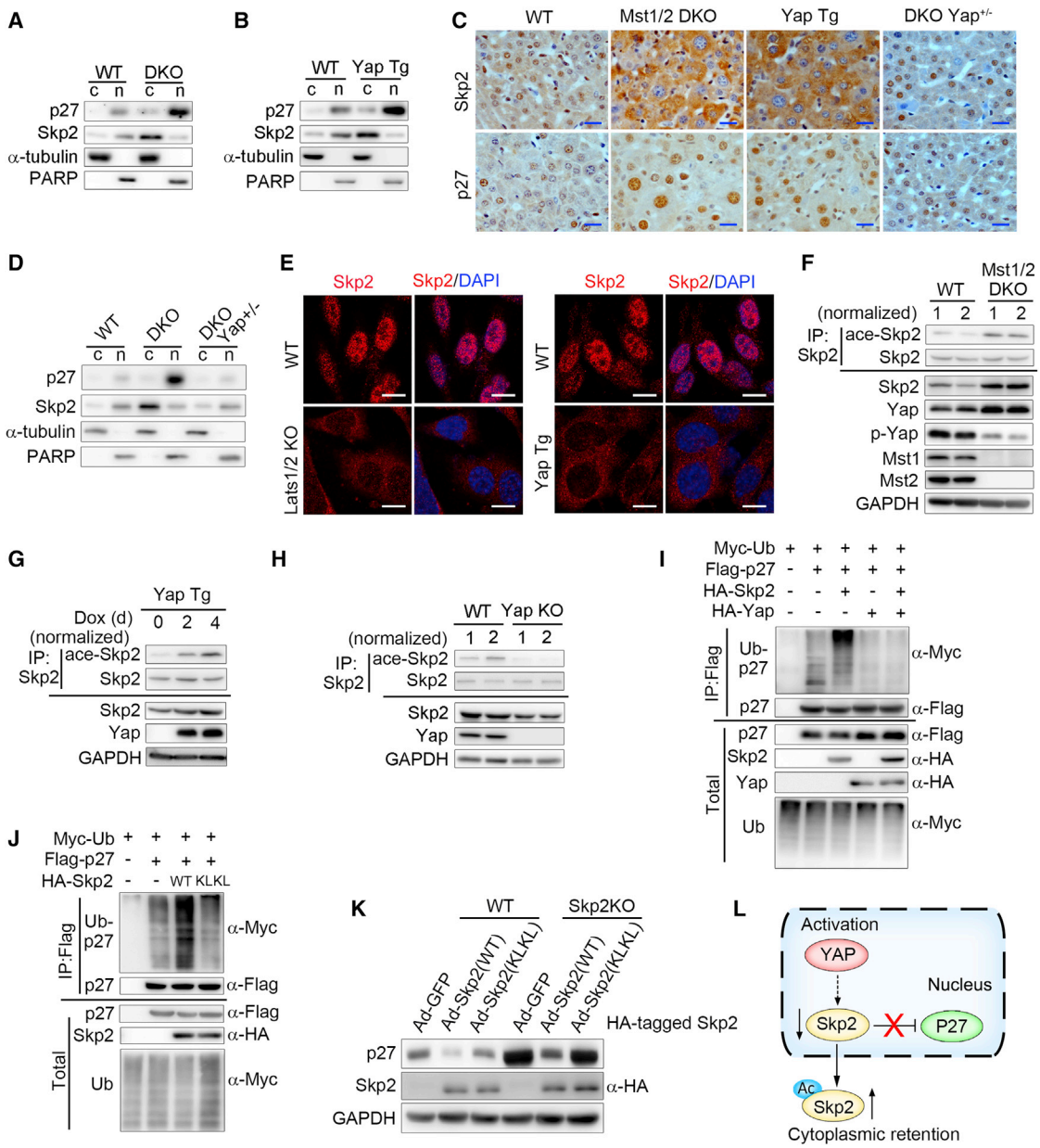

Figure 3. Loss of Hippo Signaling Enhances the Cytoplasmic Retention of Skp2

(A and B) Immunoblot analysis of p27, Skp2, α-tubulin, or PARP in the cytoplasmic (c) and nuclear (n) fractions of WT, Mst1/2 DKO (A) or Yap Tg (B) liver tissues.

(C and D) IHC staining (C) or immunoblot analysis of the cell fractions (D) of Skp2 and p27 in liver tissues from WT, Mst1/2 DKO, *Mst1*$^{f/f}$*Mst2*$^{f/f}$ *Yap*$^{+/fl}$*Alb*-Cre (DKO Yap$^{+/-}$), or Yap Tg mice. Scale bars, 20 μm.

(E) Immunofluorescent staining of Skp2 (red) and the nuclear counterstain (DAPI, blue) in primary MEFs isolated from WT, Lats1/2 KO (left panel), or Yap Tg (right panel) mice. Scale bars, 10 μm.

(F–H) Immunoblot analysis of acetylated (ace-) Skp2, Skp2, p-Yap, Yap, Mst1, Mst2, and GAPDH in the immunoprecipitates or total lysates of hepatocytes isolated from WT, Mst1/2 DKO (F), Yap Tg (G), or Yap KO (H) mice. For the detection of ace-Skp2, the loading of the immunoprecipitates was normalized according to the levels of total Skp2.

(I and J) Immunoassay assessing the ubiquitination of p27 (detected with anti-Myc) in the lysates of 293T cells expressing various combinations of Myc-tagged ubiquitin, Flag-tagged p27, HA-tagged Yap, and HA-tagged WT Skp2 (I) or an acetylation-mimetic (KLKL) mutant form of Skp2 (J) as indicated.

(K) Immunoblot analysis of Skp2, p27, and GAPDH in liver tissues from WT and Skp2 KO mice infected with Ad-GFP, Ad-Skp2 (WT), or Ad-Skp2 (KLKL).

(L) A proposed working model for Yap activation regulating p27 stability through modulating Skp2 acetylation and sub-cellular localization.

See also Figure S3.

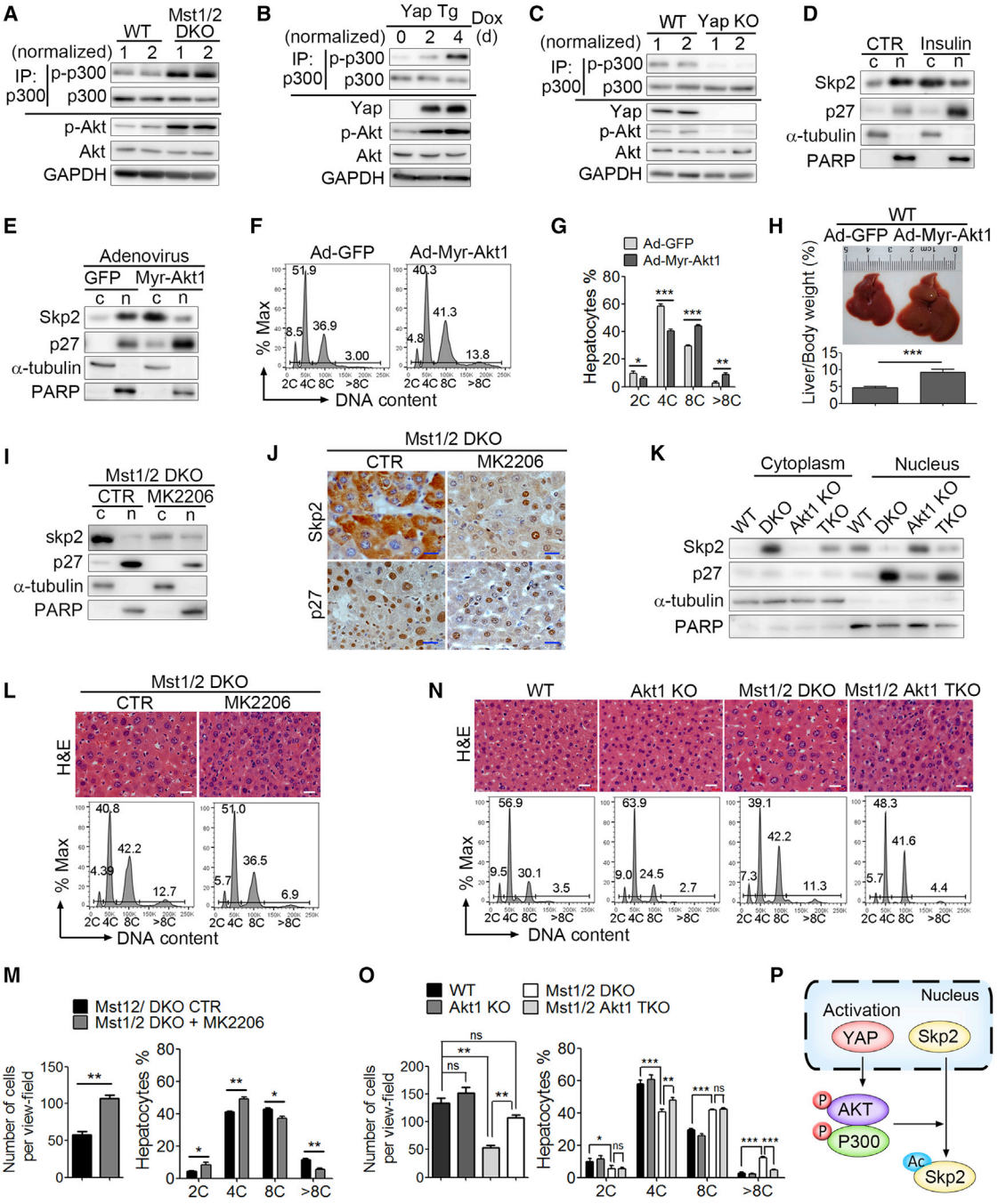

Figure 4. Yap Regulates Skp2 Cytoplasmic Retention via the Akt-p300 Axis

(A–C) Immunoblot analysis of p-p300, p300, p-Akt, Akt, Yap, or GAPDH in the immunoprecipitates or total lysates of hepatocytes isolated from WT, Mst1/2 DKO (A), Yap Tg (B), or Yap KO (C) mice. For the detection of the p-p300 levels, the loading of the immunoprecipitates was normalized according to the levels of total p300.

(D and E) Immunoblot analysis of p27, Skp2, α-tubulin, or PARP in the cytoplasmic (c) and nuclear (n) fractions of liver cells isolated from mice treated with vehicle or insulin (D) or mice infected with Ad-GFP or Ad-Myr-Akt1 (active Akt1) (E).

(F and G) FACS analysis (F) and the DNA content quantification (G) of ploidy hepatocytes from WT mice infected with Ad-GFP or Ad-Myr-Akt1 (n = 3).

(H) A representative liver picture and the liver-to-body weight ratios of WT mice (n = 5) infected with Ad-GFP or Ad-Myr-Akt1.

(I and J) Immunoblot analysis of the cell fractions (I) or IHC staining (J) of Skp2 and p27 from liver tissues isolated from Mst1/2 DKO mice treated with vehicle or the Akt inhibitor MK2206. Scale bars, 20 μm.

(K) Immunoblot analysis of Skp2, p27, α-tubulin, or PARP in the cytoplasmic and nuclear fractions of liver tissues from WT, Akt1 KO, Mst1/2 DKO, or *Mst1*$^{f/f}$ *Mst2*$^{f/f}$*Akt1 KO Alb*-Cre (triple knockout [TKO]) mice.

(legend continued on next page)

p27 in Mst1/2 DKO livers slightly increased the number of BrdU-positive hepatocytes, but dramatically increased pHH3-positive hepatocytes. This finding indicated that more cells entered mitosis for proliferation and division (Figures 2I and 2J). Furthermore, we knocked down p27 expression in WT and Mst1/2 DKO livers using adeno-associated virus (AAV), which can have a long-term effect of up to 6 months. We found that knocking down p27 in Hippo-deficient livers resulted in decreased cell polyploidy and significantly reduced the number and volume of tumor size at 5 weeks post-infection with AAV p27 shRNA (Figures 2K–2M and S2H). We found similar results in *Mst1*$^{f/f}$*Mst2*$^{f/f}$*Alb*-Cre mice with one *p27* allele deletion (Mst1/2 DKO p27$^{+/-}$) (Figures S2I–S2N). We further observed much lower incidences of abnormal anaphase cells in the livers of Mst1/2 DKO p27$^{+/-}$ mice than in Mst1/2 DKO livers, indicating that p27 downregulation restored cellular cytokinesis to normal levels in Mst1/2 DKO livers (Figures S2K and S2L). As the mitosis of polyploid cells leads to genomic instability and a higher incidence of cancer formation, it is not surprising that we observed that the loss of p27 resulted in a lower incidence and delayed tumor formation in Hippo signal-deficient livers by reducing cell polyploidy in the context of a much higher fraction of polyploid cells in Mst1/2 DKO liver tissues, although p27 downregulation increased the cell mitosis and proliferation of diploid cells (Figures 2L, 2M, S2M, and S2N). These results indicated that the Hippo signaling pathway limits polyploidy formation and prevents tumor formation, at least in part, through the downregulation of p27 (Figure 2N).

Hippo Signaling Deficiency Enhances the Cytoplasmic Retention of Skp2

Previous studies showed that S-phase kinase-associated protein 2 (Skp2) in the nuclear compartment is required for ubiquitin-mediated p27 degradation. We measured the levels of Skp2 and p27 in whole-cell lysates, and the cytoplasmic and nuclear fractions from WT, Mst1/2 DKO, or Yap Tg hepatocytes, and found that the protein levels of Skp2 and p27 were increased in whole-cell lysates of Mst1/2 DKO or Yap Tg hepatocytes compared with those in WT cells (Figures S3A and S3B). However, these proteins were present in distinct sub-cellular locations (Figures 3A and 3B). The cytoplasmic retention of Skp2 in Mst1/2 DKO or Yap Tg livers was further confirmed by immunohistochemistry (IHC) staining (Figures 3C and 3D) and was observed in primary MEFs isolated from Lats1/2 DKO or Yap Tg mice (Figure 3E) and a HepG2 cell line overexpressing Yap (Figure S3C). Furthermore, the loss of one allele of Yap in Mst1/2 DKO hepatocytes restored the nuclear localization of Skp2, thereby reducing the p27 levels (Figures 3C and 3D). These data suggested that loss of Hippo signaling resulted in the cytoplasmic retention of Skp2, leading to the nuclear accumulation of p27. Previous studies showed that the acetylation of Skp2 promotes its translocation from the nuclei to the cytosol (Inuzuka et al., 2012). In line with its sub-cellular localization, Skp2 acetylation levels were greatly increased in Mst1/2 DKO and Yap Tg hepatocytes, and attenuated in Yap KO hepatocytes (Figures 3F–3H). In addition, p27 ubiquitination was remarkably attenuated in cells overexpressing Yap or an acetylation-mimetic mutant Skp2 (KLKL) that was mainly located in the cytosol (Figures 3I and 3J). Consistently, the p27 levels were greatly reduced in Skp2 KO livers infected with adenoviruses expressing WT Skp2, but only slightly reduced in Skp2 KO liver infected with acetylation-mimetic mutant Skp2 (Ad-Skp2 [KLKL]) (Figure 3K). These results indicated that Hippo signaling regulates p27 stability through modulating Skp2 acetylation and sub-cellular localization (Figure 3L).

Yap Promotes Skp2 Cytoplasmic Retention and Hepatocyte Polyploidy via the Akt-p300 Axis

It has been reported that Yap activates the PI3K-Akt pathway (Tumaneng et al., 2012). Akt can phosphorylate and activate the acetyltransferases p300 to enhance Skp2 acetylation at both K68 and K71, which promotes Skp2 cytoplasmic translocation and protein stability (Inuzuka et al., 2012). Indeed, the phosphorylation levels of Akt and p300 were attenuated in Yap KO cells, but greatly increased in WW45 KO, Mst1/2 DKO, Lats1/2 DKO, and Yap Tg hepatocytes (Figures 4A–4C, S4A, and S4B), in which enhanced acetylation and cytoplasmic retention of Skp2 was found (Figures 3F and 3G). A previous study showed that the insulin signal activates the PI3K/Akt pathway to promote the hepatocyte tetraploidization process (Celton-Morizur et al., 2009). Interestingly, we found that insulin treatment resulted in increased cytoplasmic Skp2 and nuclear p27 levels in the liver cells, suggesting that insulin-mediated Akt activation may induce hepatocyte polyploidy by promoting the cytoplasmic retention of Skp2 (Figures 4D, S4C, and S4D). To further validate this speculation, we infected WT mice with adenovirus expressing a constitutively active myristoylated Akt1 (Ad-Myr-Akt1) or a control Ad-GFP. To avoid fatty liver induced by myr-Akt overexpression (Ono et al., 2003), the virus was titrated and a moderate titer of the virus was used. Compared with control animals infected with Ad-GFP, mice infected with Ad-Myr-Akt1 exhibited enhanced acetylation and cytoplasmic retention of Skp2 in hepatocytes, and increased hepatocyte polyploidy and liver mass (Figures 4E–4H and S4E). Furthermore, treatment with the Akt inhibitor MK2206 or the genetic disruption of Akt1 reduced the protein levels of total and cytoplasmic Skp2 and nuclear p27 in Mst1/2 DKO liver cells (Figures 4I–4K and S4F–S4G), resulting in significantly reduced hepatocyte polyploidy in Mst1/2 DKO mice (Figures 4L–4O). Taken together, these data indicated that Hippo signaling controls cell polyploidy through Akt-Skp2 signaling (Figure 4P).

Cytoplasmic Skp2 Potentiates Polyploidy Cell Proliferation and Division

To further determine whether the cytoplasmic retention of Skp2 is responsible for the high cell polyploidy profiles in

(L–O) H&E staining of liver sections (L and N, upper panel), the quantification of cell number per view field (M and O), or the DNA content quantification by FACS (L and N, lower panel, M and O) of polyploid hepatocytes from Mst1/2 DKO mice treated with the Akt inhibitor MK2206 (n = 3) (L and M) or from WT, Akt1 KO, Mst1/2 DKO, or Mst1/2 Akt1 TKO mice (n = 3) (N and O). Scale bars, 20 μm.

(P) A proposed working model for Yap activation modulating Skp2 acetylation and sub-cellular localization via Akt-P300 signaling.

Data were assessed by Student's t test and represented as mean ± SD. ns, not significant ($p > 0.05$), *$p < 0.05$; **$p < 0.01$; ***$p < 0.001$ compared between the indicated groups. See also Figure S4.

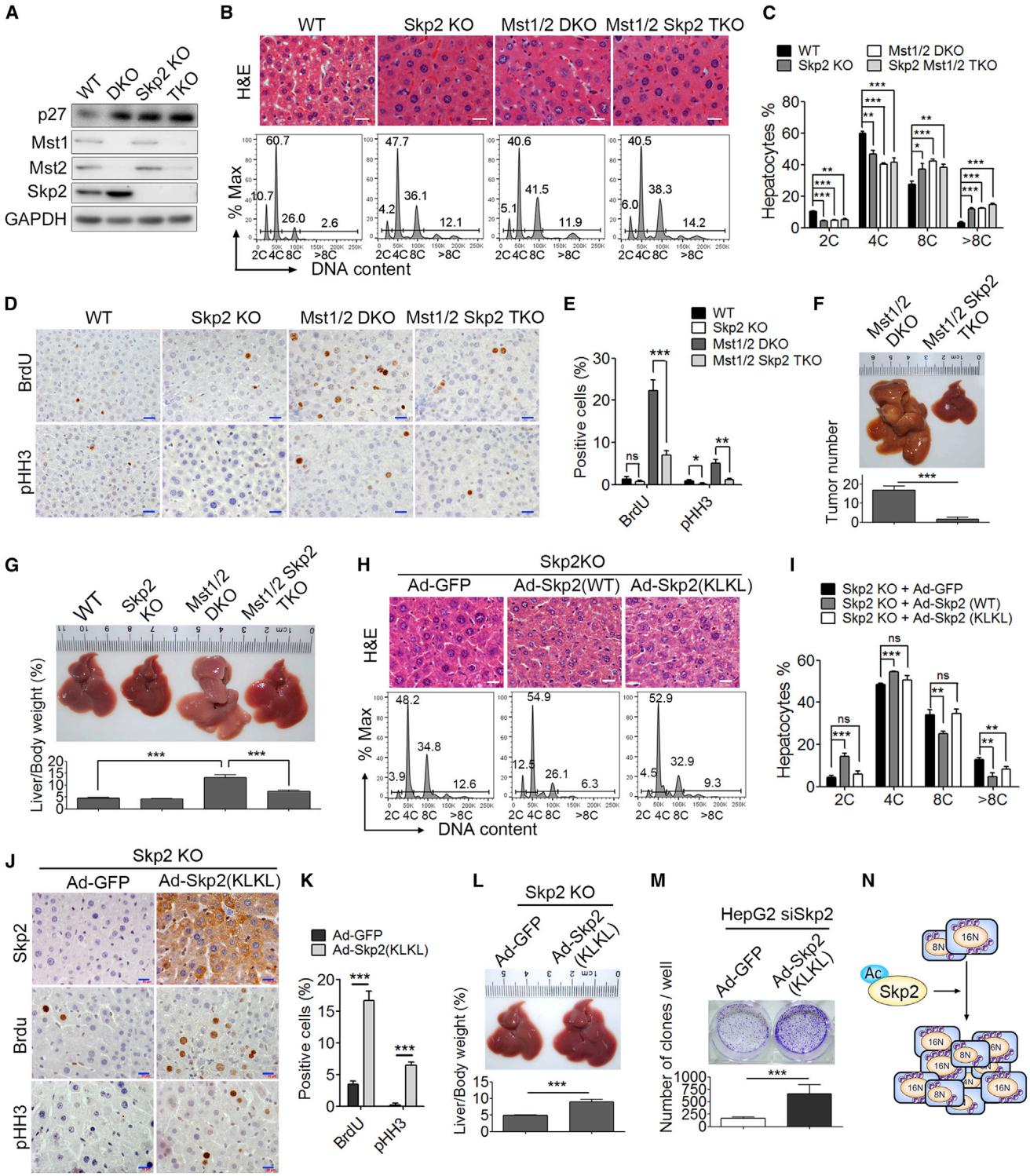

Figure 5. Cytoplasmic Skp2 Promotes Polyploid Cell Division

(A) Immunoblot analysis of p27, Skp2, Mst1, Mst2, and GAPDH in liver lysates of WT, Skp2 KO, Mst1/2 DKO, or *Mst1*$^{f/f}$*Mst2*$^{f/f}$*Skp2 KO Alb*-Cre (Mst1/2 Skp2 TKO) mice.

(B and C) H&E staining of the liver sections (B, upper panel) and the DNA content quantification of hepatocytes of the indicated mice using FACS (n = 3) (B, lower panel), and (C). Scale bars, 20 μm.

(D and E) IHC staining (D) and the quantification (E) of BrdU- or pHH3-positive cells in the liver sections from the indicated mice. Scale bars, 20 μm.

(F and G) A representative liver picture and the liver-to-body weight ratios (n = 5, 3 months old) (F) and the quantification of liver tumors (n = 5, 5 months old) (G) of the indicated mice.

(legend continued on next page)

Hippo-deficient livers, we knocked out Skp2 in Mst1/2 or WW45 KO mice. We found that the loss of Skp2 in Mst1/2 DKO or WW45 KO livers resulted in a slight increase in the p27 protein levels (Figures 5A and S5A), but had no significant effect on the cell polyploidy profiles (Figures 5B, 5C, S5B, and S5C). Interestingly, the loss of Skp2 in Mst1/2 or WW45 KO mice resulted in a dramatically decreased hepatocyte proliferation rate, a smaller liver mass, lower liver-to-body weight ratios, and fewer liver tumors (Figures 5F–5I and S5F–S5I). In contrast, the overexpression of WT Skp2, which is mainly located in the nucleus, dramatically decreased the level of nuclear p27 and resulted in significantly lower numbers of polyploid cells in both WT and Skp2 KO livers. However, the overexpression of activated Skp2 (KLKL), which is mainly located in the cytoplasm, resulted in only a slightly reduced p27 level (Figure 3K) and thus had no significant effect on the cell polyploidy profiles (Figures 5D, 5E, S5D, and S5E). Based on these observations, we speculated that cytoplasmic Skp2 in Hippo signal-deficient cells might also promote polyploidy liver cell division in addition to inducing p27-mediated cell polyploidy. Indeed, Skp2 KO mice infected with Ad-Skp2 (KLKL) exhibited a significantly increased number of BrdU-positive hepatocytes and pHH3-positive hepatocytes, indicating that more cells enter mitosis for proliferation and division (Figures 5J and 5K). Consistently, Skp2 KO mice infected with Ad-Skp2 (KLKL) had a larger liver mass and greater liver/body weight ratios than control mice that received Ad-GFP (Figure 5L). Furthermore, the expression of Ad-Skp2 (KLKL) in HepG2 cells pretreated with Skp2 siRNA (siSkp2) significantly increased its colony formation rate compared with Ad-GFP-infected control cells (Figure 5M). These results suggested that cytoplasmic Skp2 promotes polyploidy cell proliferation and division (Figure 5N).

Cytoplasmic Skp2 Degrades FoxOs to Enhance Polyploid Cell Proliferation and Division

The data above suggested that cytoplasmic Skp2 might have other downstream effectors to regulate cell proliferation and liver size. Previous studies have shown that, in contrast to nuclear Skp2, which targets nuclear p27 as shown above, cytoplasmic Skp2 has a distinct set of substrates, including forkhead box O (FoxO) transcription factors, which are important pro-apoptotic transcription factors that block cellular proliferation, promote cell death, and drive cells into a quiescent state (Huang et al., 2005). Indeed, we found that, compared with WT controls, the total protein levels of FoxO1/3 and the mRNA expression levels of the FoxO1/3 target genes, such as *Sod2*, *Catalase*, *G6pase*, *Pepck*, *Ang2*, *Fasl*, *Bnip3*, *Ccng2*, and *Igfbp1*, were dramatically reduced in Mst1/2 DKO and Yap Tg livers, indicating the attenuated function of FoxO1/3 in Hippo-deficient livers (Figures 6A, 6B, S6A, and S6B). Consistently, the genetic disruption of Skp2 increased the protein levels of FoxO1 and FoxO3a in both WT and Mst1/2 DKO mouse livers (Figure 6C). Previous studies established the mechanism of FoxO inhibition in which Akt kinases phosphorylate FoxO1 at Thr24, Ser256, and Ser319, or FoxO3 at Thr32 and Ser253, thereby increasing their association with 14-3-3 proteins (Tran et al., 2003). This, in turn, results in the translocation of FoxO proteins from the nucleus to the cytoplasm, leading to their transcriptional inactivation. In fact, we found that the increased phosphorylation levels of FoxO1(S256, T24) and FoxO3a(T32) correlated with enhanced Akt activity in Mst1/2 DKO and Yap Tg liver lysates (Figures 6D and S6C). Immunoblotting of sub-cellular fractions or IHC staining assays further confirmed that, compared with WT controls, the FoxO1/3 protein levels were dramatically reduced in the nuclear fractions of Mst1/2 DKO or Yap Tg liver cells (Figure 6E, 6F, and S6D), and the total protein level and sub-cellular distribution of FoxO1/3 were restored to relatively normal levels in Mst1/2 DKO $Yap^{+/-}$ liver cells (Figures 6E and 6F). Consistently, inhibition or genetic disruption of Akt reduced the FoxO1/3 phosphorylation levels and restored FoxO1/3 protein levels and the sub-cellular distribution in Mst1/2 DKO and Yap Tg livers (Figures 6D, 6G, and S6C). Furthermore, Skp2-mediated FoxO ubiquitination was remarkably enhanced in cells overexpressing Yap, while Akt inhibition attenuated this effect (Figures 6H and 6I). Based on these results, we speculated that cytoplasmic Skp2-mediated FoxO1/3 degradation might be required for Hippo signal-deficient polyploid cell survival and proliferation. To examine this possibility, we reintroduced the non-degradable form of FoxO1(S256A) in Mst1/2 DKO or Yap Tg livers using adenoviral vectors, Ad-FoxO1(S256A). Importantly, Ad-FoxO1(S256A) greatly blocked cell proliferation, enhanced cell apoptosis, and reduced liver mass compared with those in control mice receiving Ad-GFP (Figures 6J, 6K, and S6E). Notably, Ad-FoxO1(S256A) abrogated the Ad-Skp2 (KLKL)-driven Skp2-deficient liver overgrowth (Figure 6L). These data indicated that the loss of Hippo signaling promotes polyploid cell division and oncogenesis, at least in part, through Skp2-mediated FoxO1/3 degradation (Figure 6M).

Yap-Akt-Skp2 Signaling Is Implicated in Human HCC Development

The data above demonstrated that the loss of Hippo signaling in the liver resulted in the cytoplasmic retention of both Skp2 and FoxO through the activation of Akt, which promotes Skp2-mediated FoxO degradation, thereby enhancing p27-induced polyploid cell division, genomic instability, and oncogenesis.

(H and I) H&E staining of the liver sections from Skp2 KO mice infected with Ad-GFP, Ad-Skp2 (WT), or Ad-Skp2 (KLKL) (H, upper panel) and the DNA content quantification of hepatocytes from the indicated mice using FACS (n = 3) (H, lower panel, and I). Scale bars, 20 μm.

(J and K) IHC staining of BrdU or pHH3 (J) and the quantification of BrdU- or pHH3-positive cells (K) in liver sections from Skp2 KO mice infected with adenovirus Ad-GFP or Ad-Skp2 (KLKL) (n = 3). Scale bars, 20 μm.

(L) The representative liver sizes and liver-to-body weight ratios (n = 5) of Skp2 KO mice infected with Ad-GFP or AD-Skp2 (KLKL).

(M) A representative image of the clonogenic assay and the quantification of clones per well for Skp2-knocked down HepG2 cells infected with Ad-GFP or Ad-Skp2 (KLKL).

(N) A proposed working model for acetylated Skp2 promoting liver polyploidy cell proliferation.

Data were assessed by Student's t test and represented as mean ± SD. ns, not significant ($p > 0.05$), *$p < 0.05$, **$p < 0.01$, ***$p < 0.001$ compared between the indicated groups. See also Figure S5.

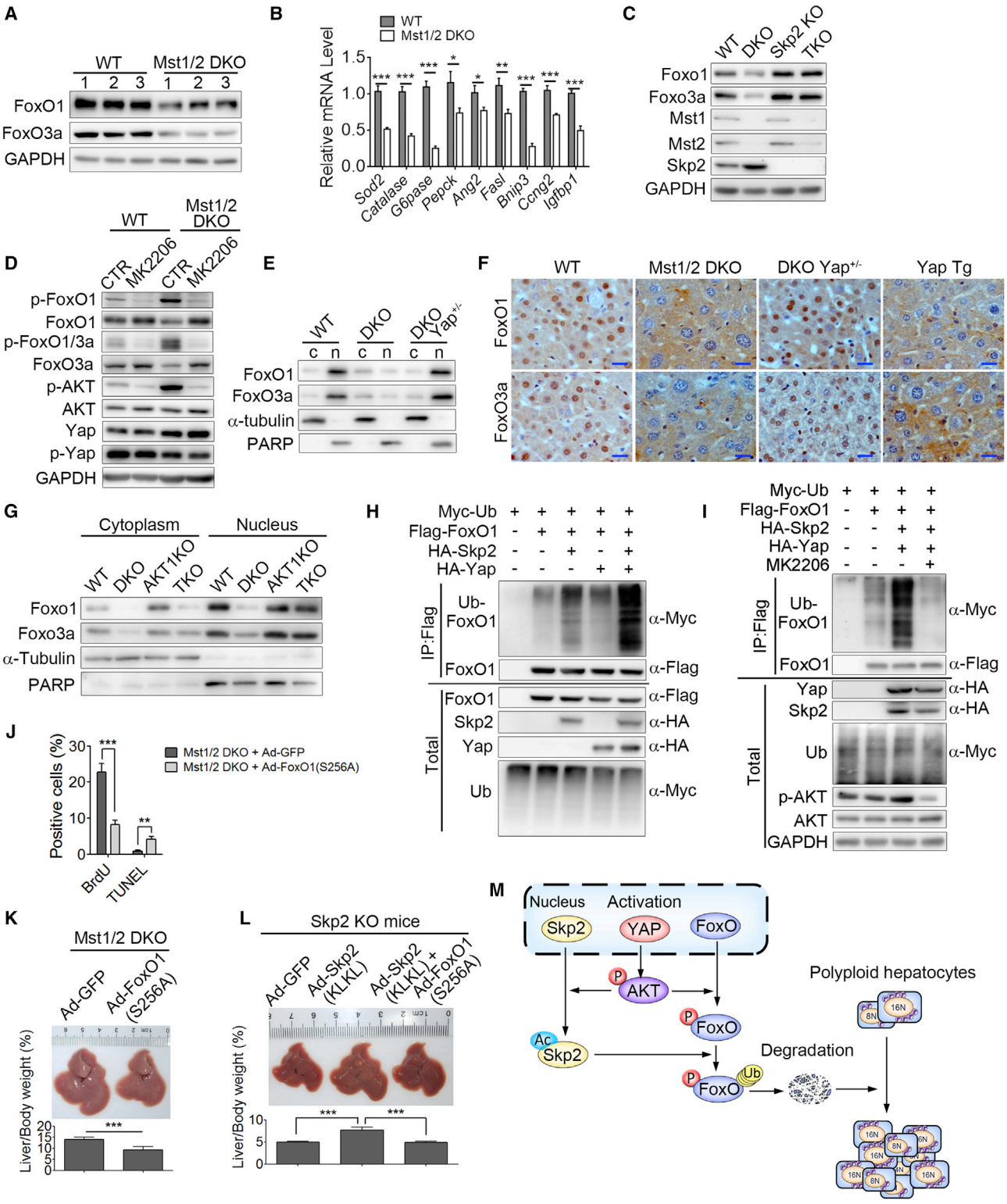

Figure 6. Yap Promotes Polyploid Cell Division via Skp2-Mediated FoxO Degradation

(A and B) Immunoblot analysis of FoxO1, FoxO3a, and GAPDH (A) and qPCR analysis of FoxO target genes (B) in liver of WT or Mst1/2 DKO mice.

(C) Immunoblot analysis of FoxO1, FoxO3a, Mst1, Mst2, Skp2, and GAPDH in WT, Mst1/2 DKO, Skp2 KO, or *Mst1*$^{f/f}$*Mst2*$^{f/f}$*Skp2 KO Alb*-Cre (TKO) liver lysates.

(D) Immunoblot analysis of p-FoxO1 (S256), p-FoxO1/3 (T24/T32), p-Akt, p-Yap, FoxO1, FoxO3a, Akt, Yap, and GAPDH in liver lysates of WT or Mst1/2 DKO mice treated with vehicle control (CTR) or Akt inhibitor MK2206.

(legend continued on next page)

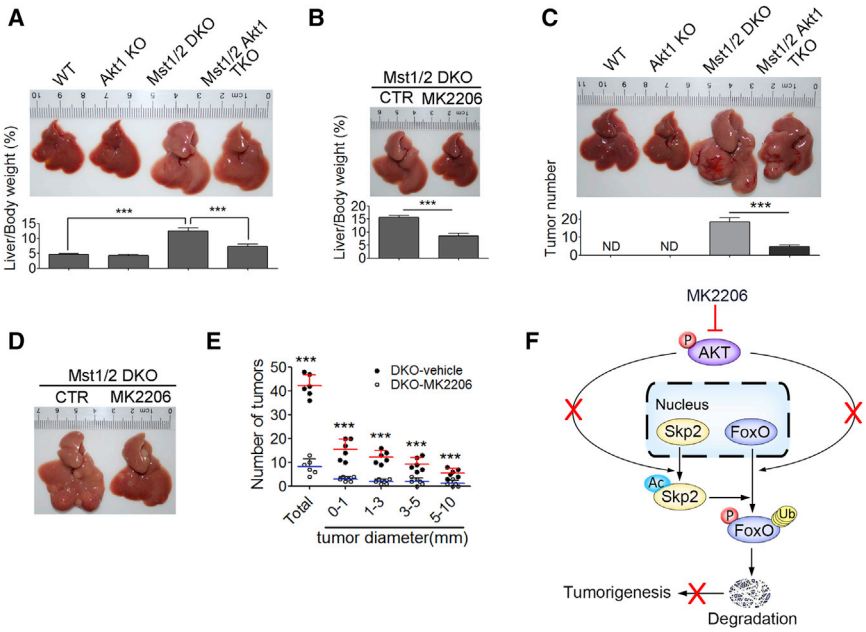

Figure 7. Disruption of Akt Function Attenuates Liver Tumor Formation in Mst1/2 DKO Mice

(A and B) Representative liver pictures and the liver-to-body weight ratios of Mst1/2 DKO mice treated with the Akt inhibitor MK2206 (n = 5) (A) or of WT, Akt1 KO, Mst1/2 DKO, or Mst1/2 Akt1 TKO mice (n = 5) (B).

(C) A representative liver picture and the quantification of tumor number from WT, Akt1 KO, Mst1/2 DKO, or Mst1/2 Akt1 TKO mice (n = 6).

(D and E) A representative liver picture and the quantification of the size and number of liver tumors (n = 6) of 5-month-old Mst1/2 DKO mice treated with vehicle or the Akt inhibitor MK2206.

(F) A proposed working model for the disruption of Akt function attenuating liver tumor formation in Mst1/2 DKO mice.

Data were assessed by Student's t test and represented as mean ± SD. ***p < 0.001 compared between the indicated groups. ND, non-detectable.

Importantly, the inhibition or genetic disruption of Akt resulted in significantly reduced p27 levels, hepatocyte polyploidy, and decreased liver-to-body weight ratios for Mst1/2 DKO mice (Figures 4I–4O, 7A, and 7B). We observed that the loss of Akt1 in Mst1/2 DKO mice resulted in a significantly lower incidence of HCC in old age (Figure 7C). Consistently, Mst1/2 DKO mice that have been treated with the Akt inhibitor MK2206 exhibited a significant decrease in the size and number of tumors, which correlated with the reduced cytoplasmic Skp2 levels in liver tissues compared with control animals (Figures 7D–7F, S4E, and S4F). We then examined 60 pairs of liver-derived tumorous and adjacent non-tumorous tissues. Yap activation was associated with decreased FoxO1/3, increased Skp2 acetylation, and Akt phosphorylation in tumorous tissues compared with those in adjacent noncancerous tissues (Figures 8A–8C and S7A). These results suggested that Yap-Akt-Skp2 signaling is associated with human HCC development.

The examination of the tissue microarray of human liver tumors and adjacent non-tumorous tissues (n = 94) by IHC staining revealed that the expression levels of Yap and Skp2 were higher in cancer tissues than in adjacent noncancerous liver tissues (Figure S7B). Nuclear Yap expression and cytoplasmic Skp2 expression were primarily increased in cancer tissues compared with those in adjacent noncancerous tissues, and were associated with advanced tumor stages (Table S1; Figures 8D–8G). Furthermore, increased nuclear Yap expression in cancer tissues was associated with enhanced cytoplasmic Skp2 expression (Figure 8H, $R^2 = 0.3724$, $p < 0.0001$). Although there was no significant association between Yap or Skp2 expression and sex or age (Table S1), there was a positive correlation between the nuclear Yap expression or cytoplasmic Skp2 expression and pathological grade (Table S1). In addition, Kaplan-Meier survival analysis revealed that the survival time for patients with high nuclear Yap expression was obviously shorter than those with low Yap expression (p = 0.0275). Similarly, the cytoplasmic Skp2 expression level had a negative correlation with survival (p = 0.0185). Thus, we concluded that there is a close connection between these two proteins in human HCC development, and that the inhibition of Akt activity may be a promising therapeutic strategy to treat HCC resulting from the loss of Hippo signaling.

DISCUSSION

How diploid organisms develop polyploid cells remains largely unknown. Herein, we report that Hippo signaling maintains liver cell ploidy in a p53-independent manner. We found that Hippo signal deficiency or Yap activation turn on Akt signaling, thereby activating the acetyltransferase p300 to promote Skp2

(E and F) Immunoblot analysis of the cell fractions (E) or IHC staining (F) of FoxO1 or FoxO3a of liver cells from WT, Mst1/2 DKO, *Mst1*$^{f/f}$*Mst2*$^{f/f}$ *YAP* $^{+/fl}$*Alb*-Cre (DKO Yap$^{+/-}$), or Yap Tg mice. Scale bars, 20 μm.

(G) Immunoblot analysis of FoxO1, FoxO3a, α-tubulin, or PARP in the cytoplasmic and nuclear fractions of WT, Mst1/2 DKO, Akt1 KO, or Mst1/2 Akt1 TKO liver tissues.

(H and I) Immunoassay of the ubiquitination of FoxO1 (detected with anti-Myc) in the lysates of 293T cells expressing various combinations of Myc-tagged ubiquitin, Flag-tagged FoxO1, HA-tagged Yap, and HA-tagged Skp2 (H) with or without Akt inhibitor MK2206 treatment.

(J) Quantification of BrdU- or TUNEL-positive cells in the liver sections from Mst1/2 DKO mice infected with Ad-GFP or Ad-FoxO1(S256A) (n = 3).

(K and L) The representative liver sizes and liver-to-body weight ratios of Mst1/2 DKO infected with adenovirus Ad-GFP or Ad-FoxO1(S256A) (n = 5) (K) or Skp2 KO mice infected with adenovirus Ad-GFP, Ad-FoxO1(S256A), Ad-Skp2(KLKL), or Ad-FoxO1(S256A) plus Ad-Skp2(KLKL) (n = 5) (L).

(M) A proposed working model for Yap promoting polyploid cell division via Skp2-mediated FoxO degradation.

Data were assessed by Student's t test and represented as mean ± SD. *p < 0.05, **p < 0.01, ***p < 0.001 compared between the indicated groups. See also Figure S6.

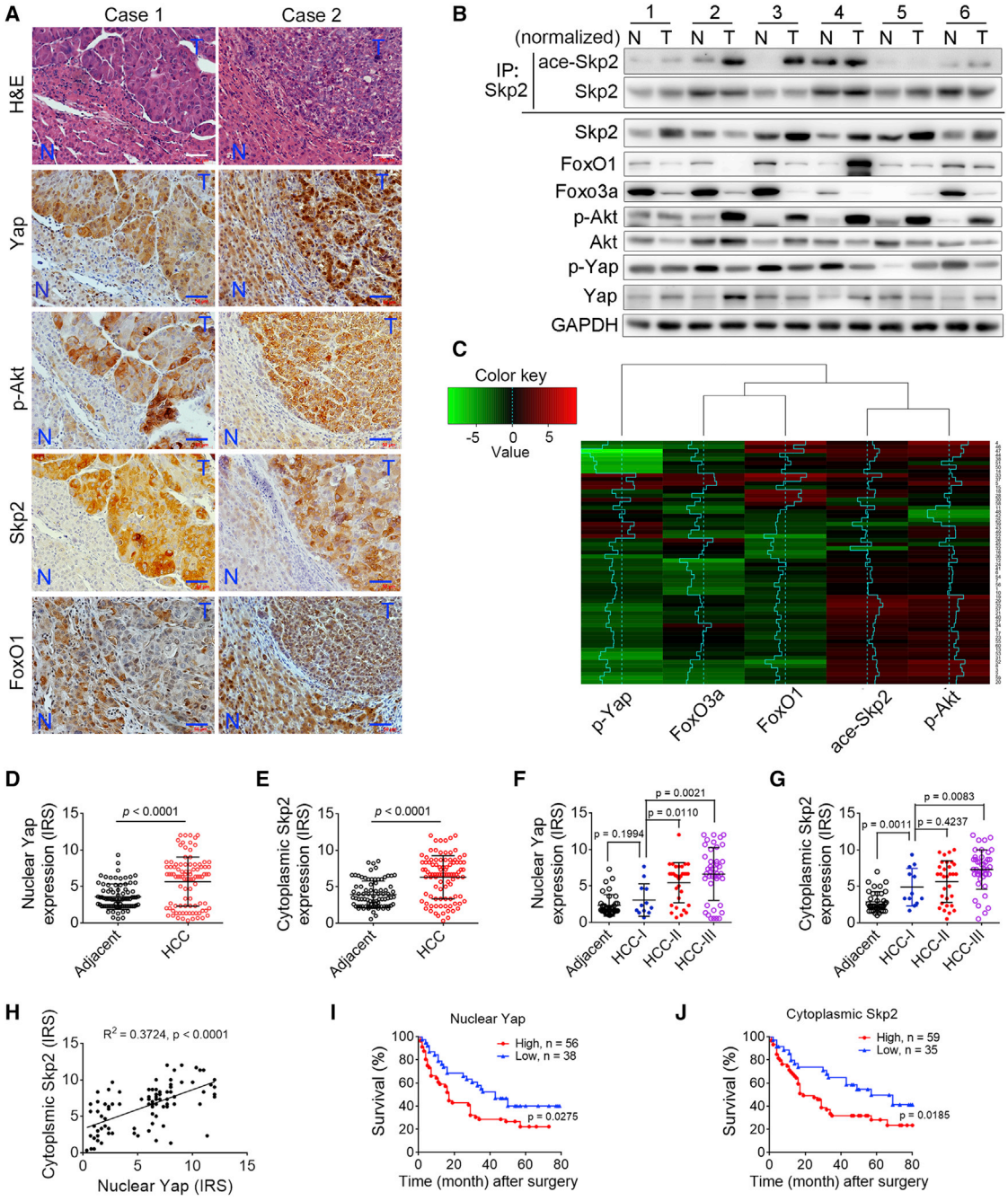

Figure 8. Yap-Akt-Skp2 Signal Is Implicated in Human HCC Progress

(A) A representative image of H&E staining and the IHC analysis of p-Yap, p-Akt, Skp2, or FoxO1 in the liver sections of adjacent non-tumorous livers (N) or HCC tissues (T) isolated from one patient. Scale bars, 50 μm.

(B and C) Western blot analysis of ace-Skp2, Skp2, FoxO1, FoxO3a, p-Akt, Akt, p-Yap, Yap and GAPDH in HCC tissue (T) and adjacent non-tumorous liver tissue (N) isolated from one patient. Six representative paired samples are shown (B). See Figure S7A for the remaining 54 paired samples. For the detection of ace-Skp2, the loading of immunoprecipitates was normalized according to the levels of total Skp2. The intensities of the immunoblot bands were quantified using ImageJ software. A heatmap representation of the ratio of the relative expression of the proteins p-Yap, FoxO3a, FoxO1, ace-Skp2, or p-Akt in the T and N samples from one patient. Clustering was performed by using Pearson correlation metric and centroid linkage (C).

(D–G) Scatterplot analysis of the immunoreactive score (IRS) of the nuclear Yap (D and F) or the cytoplasmic skp2 (E and G) impaired liver cancer and adjacent non-cancer paraffin tissue sections or in different tumor stages from the tissue microarray of human liver cancer. IRS scores of 0–1 indicate negative; scores of 2–3 indicate mild; scores of 4–8 indicate moderate; scores of 9–12 indicate strongly positive. A total of 94 paired samples are shown. The data were assessed by Student's t test and are represented as the mean ± SD.

(legend continued on next page)

acetylation, stabilization, and cytoplasmic retention, which results in p27 hyper-accumulation and induces cell polyploidy. As a result of Skp2 cytoplasmic retention, the pro-apoptotic factors FoxO1/3 are overly degraded and thereby promote polyploid cell division, genomic instability, and oncogenesis. Moreover, the inhibition or genetic disruption of Akt or p27 reduces cell polyploidy and oncogenesis, whereas the depletion of Skp2 has no significant effect on Mst1/2-null cell polyploidy, but does prevent polyploid cell division and abrogates liver overgrowth and tumorigenesis. These data indicate that Hippo-Skp2 signaling prevents genomic instability through two possible mechanisms: maintaining Skp2-mediated p27 degradation in the nuclei to limit polyploidy formation or preventing Skp2-mediated FoxO1/3 degradation in the cytosol to block polyploidy cell division, thereby limiting the risk of genomic instability, aneuploidy, and tumorigenesis.

Our current study demonstrates that the sustained activation of Yap overrides the p27-mediated checkpoint, at least in part, through the degradation of FoxO family proteins, allowing polyploid cells to proliferate inappropriately with mitotic defects and resulting in centrosome amplification, genomic instability, and cell oncogenesis. In fact, p27 plays a dual role in the regulation of the cell cycle and genomic stability in the mouse liver (Carrano et al., 1999; Kossatz et al., 2004; Nakayama et al., 2004; Serres et al., 2012). For cell-cycle control, elevated p27 arrests the cell cycle via the inhibition of CDKs to prevent cell division. In contrast, increased p27 results in mitotic defects and promotes endoreduplication cycles to induce cell polyploidy and genomic instability in mouse livers, while a loss of p27 reduces cell polyploidy, thereby maintaining genomic stability. In addition, p27 has long been known to be an assembly factor for cyclin D/Cdk4 complexes (LaBaer et al., 1997). Thus, elevated p27 in polyploid cells might increase Cdk4 activity and promote cell division, aneuploidy, and genomic instability, thus contributing to the development of cancer. In the context of the much higher fraction of polyploid cells in Mst1/2 DKO liver tissues, it is not surprising to observe that the loss of p27 in Hippo-deficient livers resulted in decreased cell polyploidy and a significantly reduced number and volume of tumor size. Thus, these data support a key role of p27 expression in the tumorigenesis of polyploid organs, such as livers with deregulated Hippo signaling.

Previous studies have shown that tetraploid cells arrest their cell cycle in a p53-dependent manner. Hippo tumor suppressor pathway Lats1/2 kinases were shown to induce tetraploid cell-cycle arrest by preventing Mdm2-mediated p53 degradation (Aylon et al., 2006; Iida et al., 2004; McPherson et al., 2004). However, we found that Yap overexpression or the deletion of Yap inhibitory components such as WW45, Mst1/2, and Lats1/2 in mouse livers results in highly increased p53 expression and activity. Moreover, the combined losses of Hippo signaling and p53 lead to greatly increased polyploidy with multiple nuclei and results in a higher incidence and earlier onset of liver tumors. Thus, the increased p53-mediated response might be a potent negative feedback loop in response to increased cell polyploidy upon the disruption of Hippo signals. Alternatively, other effectors downstream of Yap that positively augment the p53 response possibly exist. These results suggested that Hippo signaling might play a dual role in p53 regulation, positively as a blockage of Mdm2-mediated p53 degradation by Lats1/2 but negatively as an inhibitor of the Yap-induced p53 response. It will be of particular interest to determine how Yap regulates p53 activity in future studies.

In addition, a previous study showed that tetraploid cells have lower Rho activity, which is mainly due to increased Rac activation in the presence of excess microtubules nucleated by extra centrosomes (Ganem et al., 2014). Restoring Rho activity enables the cell to bypass G1 arrest. Consistently, enhanced cell-matrix adhesion, which activates Rho, is reported to reduce the G1 arrest of tetraploid cells. Interestingly, our previous work demonstrated that the Hippo kinases Mst1 and Mst2 are required for Rac activation (Geng et al., 2015). Thus, whether the reintroduction of active Rac induces the G1 arrest of tetraploid cells is an interesting open question. Moreover, a previous study reported that Mst1 limits the kinase activity of aurora B to promote stable kinetochore-microtubule attachment (Oh et al., 2010). Thus, there might be other effectors downstream of Hippo signaling that mediate polyploidy. In conclusion, our results reveal that the modulation of the Hippo signaling pathway orients hepatocytes into a specific cell-cycle program, leading to the generation of diploid or polyploid cells. It is of interest to determine whether Hippo signaling is also involved in the regulation of other polyploid cell types such as megakaryocyte polyploidization.

STAR★METHODS

Detailed methods are provided in the online version of this paper and include the following:

- KEY RESOURCES TABLE
- CONTACT FOR REAGENT AND RESOURCE SHARING
- EXPERIMENTAL MODEL AND SUBJECT DETAILS
  - Mice
  - Cell Lines and Cell Culturing
  - Human Liver and HCC Samples
- METHOD DETAILS
  - Hepatocyte Isolation and Ploidy Measurement
  - Correlation Analysis of Cell Size, Nucleus Size and DNA Content
  - MEF Preparation and Infection
  - Hydrodynamic Gene Delivery
  - Generation of Recombinant Adenovirus
  - shRNA and Lentiviral Infection
  - Generation of AAV-Shp27 Virus
  - Real-Time Quantitative PCR
  - SDS-PAGE and Immunoblot Analysis
  - Immunofluorescence Staining

(H) The IRS of nuclear Yap and the cytoplasmic Skp2 of liver cancer sections from the tissue microarray of human liver cancer was plotted and assessed using a linear regression t test.

(I and J) Kaplan-Meier plot of overall survival of patients with HCC stratified by high IRS (>6) or low IRS (<6) of nuclear Yap (I) or cytoplasmic Skp2 (J) expression levels. A log-rank test is used for statistical analysis. See also Figure S7 and Table S1.

- Immunohistochemistry
- Clonogenic Assay for the Cell-Survival Experiment
- Treatment of Mice with Akt Inhibitor MK2206

● QUANTIFICATION AND STATISTICAL ANALYSIS

SUPPLEMENTAL INFORMATION

Supplemental Information includes seven figures and one table and can be found with this article online at http://dx.doi.org/10.1016/j.ccell.2017.04.004.

AUTHOR CONTRIBUTIONS

D.Z. and L.C. conceived the project with the input from D.G., L.Z., Q.W., X.D., and K.-H.L. S.Z., Q.C., Q.L., Y.L., X.S., L.H., S.J., C.L., J.G., W.Z., Z.L., Y.Z., D.G., and Q.L. performed experimental biological research. Z.-Y.Y. provided human HCC samples. R.-L.J., K.N., K.-I.N., Z.L., and L.Z. provided mutant mice. L.C. and D.Z. co-wrote the paper. All authors edited the manuscript.

ACKNOWLEDGMENTS

The Yap (S127A) transgenic mice were kindly provided by Dr. Fernando Camargo from Harvard Medical School, Boston, MA. D.Z. and L.C. were supported by the National Natural Science Foundation of China (31625010, U1505224, and J1310027 to D.Z.; 81422018, U1405225, and 81372617 to L.C.; 81472229 to L.H.), the National Basic Research Program (973) of China (2015CB910502 to L.C.), the Fundamental Research Funds for the Central Universities of China-Xiamen University (20720140551 to L.C. and 2013121034 and 20720140537 to D.Z.). The funders had no role in study design, data collection and analysis, decision to publish, or preparation of the manuscript.

Received: May 23, 2016
Revised: November 15, 2016
Accepted: April 5, 2017
Published: May 8, 2017

REFERENCES

Aylon, Y., Michael, D., Shmueli, A., Yabuta, N., Nojima, H., and Oren, M. (2006). A positive feedback loop between the p53 and Lats2 tumor suppressors prevents tetraploidization. Genes Dev. *20*, 2687–2700.

Beer, S., Zetterberg, A., Ihrie, R.A., McTaggart, R.A., Yang, Q., Bradon, N., Arvanitis, C., Attardi, L.D., Feng, S., Ruebner, B., et al. (2004). Developmental context determines latency of MYC-induced tumorigenesis. PLoS Biol. *2*, e332.

Calvisi, D.F., Ladu, S., Pinna, F., Frau, M., Tomasi, M.L., Sini, M., Simile, M.M., Bonelli, P., Muroni, M.R., Seddaiu, M.A., et al. (2009). SKP2 and CKS1 promote degradation of cell cycle regulators and are associated with hepatocellular carcinoma prognosis. Gastroenterology *137*, 1816–1826, e1811–1810.

Camargo, F.D., Gokhale, S., Johnnidis, J.B., Fu, D., Bell, G.W., Jaenisch, R., and Brummelkamp, T.R. (2007). YAP1 increases organ size and expands undifferentiated progenitor cells. Curr. Biol. *17*, 2054–2060.

Carrano, A.C., Eytan, E., Hershko, A., and Pagano, M. (1999). SKP2 is required for ubiquitin-mediated degradation of the CDK inhibitor p27. Nat. Cell Biol. *1*, 193–199.

Celton-Morizur, S., Merlen, G., Couton, D., Margall-Ducos, G., and Desdouets, C. (2009). The insulin/Akt pathway controls a specific cell division program that leads to generation of binucleated tetraploid liver cells in rodents. J. Clin. Invest. *119*, 1880–1887.

Chan, C.H., Li, C.F., Yang, W.L., Gao, Y., Lee, S.W., Feng, Z., Huang, H.Y., Tsai, K.K., Flores, L.G., Shao, Y., et al. (2012). The Skp2-SCF E3 ligase regulates Akt ubiquitination, glycolysis, herceptin sensitivity, and tumorigenesis. Cell *149*, 1098–1111.

Davoli, T., and de Lange, T. (2011). The causes and consequences of polyploidy in normal development and cancer. Annu. Rev. Cell Dev. Biol. *27*, 585–610.

Davoli, T., Denchi, E.L., and de Lange, T. (2010). Persistent telomere damage induces bypass of mitosis and tetraploidy. Cell *141*, 81–93.

Dong, J., Feldmann, G., Huang, J., Wu, S., Zhang, N., Comerford, S.A., Gayyed, M.F., Anders, R.A., Maitra, A., and Pan, D. (2007). Elucidation of a universal size-control mechanism in *Drosophila* and mammals. Cell *130*, 1120–1133.

Duncan, A.W. (2013). Aneuploidy, polyploidy and ploidy reversal in the liver. Semin. Cell Dev. Biol. *24*, 347–356.

Duncan, A.W., Hickey, R.D., Paulk, N.K., Culberson, A.J., Olson, S.B., Finegold, M.J., and Grompe, M. (2009). Ploidy reductions in murine fusion-derived hepatocytes. PLoS Genet. *5*, e1000385.

Duncan, A.W., Taylor, M.H., Hickey, R.D., Hanlon Newell, A.E., Lenzi, M.L., Olson, S.B., Finegold, M.J., and Grompe, M. (2010). The ploidy conveyor of mature hepatocytes as a source of genetic variation. Nature *467*, 707–710.

Dupont, S., Morsut, L., Aragona, M., Enzo, E., Giulitti, S., Cordenonsi, M., Zanconato, F., Le Digabel, J., Forcato, M., Bicciato, S., et al. (2011). Role of YAP/TAZ in mechanotransduction. Nature *474*, 179–183.

Fedchenko, N., and Reifenrath, J. (2014). Different approaches for interpretation and reporting of immunohistochemistry analysis results in the bone tissue – a review. Diagn. Pathol. *9*, 221.

Fujiwara, T., Bandi, M., Nitta, M., Ivanova, E.V., Bronson, R.T., and Pellman, D. (2005). Cytokinesis failure generating tetraploids promotes tumorigenesis in p53-null cells. Nature *437*, 1043–1047.

Ganem, N.J., and Pellman, D. (2007). Limiting the proliferation of polyploid cells. Cell *131*, 437–440.

Ganem, N.J., Cornils, H., Chiu, S.Y., O'Rourke, K.P., Arnaud, J., Yimlamai, D., Thery, M., Camargo, F.D., and Pellman, D. (2014). Cytokinesis failure triggers hippo tumor suppressor pathway activation. Cell *158*, 833–848.

Gao, D., Inuzuka, H., Tseng, A., Chin, R.Y., Toker, A., and Wei, W. (2009). Phosphorylation by Akt1 promotes cytoplasmic localization of Skp2 and impairs APCCdh1-mediated Skp2 destruction. Nat. Cell Biol. *11*, 397–408.

Geng, J., Sun, X., Wang, P., Zhang, S., Wang, X., Wu, H., Hong, L., Xie, C., Li, X., Zhao, H., et al. (2015). Kinases Mst1 and Mst2 positively regulate phagocytic induction of reactive oxygen species and bactericidal activity. Nat. Immunol. *16*, 1142–1152.

Gentric, G., and Desdouets, C. (2014). Polyploidization in liver tissue. Am. J. Pathol. *184*, 322–331.

Gordon, D.J., Resio, B., and Pellman, D. (2012). Causes and consequences of aneuploidy in cancer. Nat. Rev. Genet. *13*, 189–203.

Heallen, T., Zhang, M., Wang, J., Bonilla-Claudio, M., Klysik, E., Johnson, R.L., and Martin, J.F. (2011). Hippo pathway inhibits Wnt signaling to restrain cardiomyocyte proliferation and heart size. Science *332*, 458–461.

Hsu, S.H., Delgado, E.R., Otero, P.A., Teng, K.Y., Kutay, H., Meehan, K.M., Moroney, J.B., Monga, J.K., Hand, N.J., Friedman, J.R., et al. (2016). MicroRNA-122 regulates polyploidization in the murine liver. Hepatology *64*, 599–615.

Huang, H., Regan, K.M., Wang, F., Wang, D., Smith, D.I., van Deursen, J.M., and Tindall, D.J. (2005). Skp2 inhibits FOXO1 in tumor suppression through ubiquitin-mediated degradation. Proc. Natl. Acad. Sci. USA *102*, 1649–1654.

Iida, S., Hirota, T., Morisaki, T., Marumoto, T., Hara, T., Kuninaka, S., Honda, S., Kosai, K., Kawasuji, M., Pallas, D.C., and Saya, H. (2004). Tumor suppressor WARTS ensures genomic integrity by regulating both mitotic progression and G1 tetraploidy checkpoint function. Oncogene *23*, 5266–5274.

Inuzuka, H., Gao, D., Finley, L.W., Yang, W., Wan, L., Fukushima, H., Chin, Y.R., Zhai, B., Shaik, S., Lau, A.W., et al. (2012). Acetylation-dependent regulation of Skp2 function. Cell *150*, 179–193.

Johnson, R., and Halder, G. (2014). The two faces of Hippo: targeting the Hippo pathway for regenerative medicine and cancer treatment. Nat. Rev. Drug Discov. *13*, 63–79.

Kossatz, U., Dietrich, N., Zender, L., Buer, J., Manns, M.P., and Malek, N.P. (2004). Skp2-dependent degradation of p27kip1 is essential for cell cycle progression. Genes Dev. *18*, 2602–2607.

Kurinna, S., Stratton, S.A., Coban, Z., Schumacher, J.M., Grompe, M., Duncan, A.W., and Barton, M.C. (2013). p53 regulates a mitotic transcription program and determines ploidy in normal mouse liver. Hepatology *57*, 2004–2013.

LaBaer, J., Garrett, M.D., Stevenson, L.F., Slingerland, J.M., Sandhu, C., Chou, H.S., Fattaey, A., and Harlow, E. (1997). New functional activities for the p21 family of CDK inhibitors. Genes Dev. *11*, 847–862.

Lee, S.W., Li, C.F., Jin, G., Cai, Z., Han, F., Chan, C.H., Yang, W.L., Li, B.K., Rezaeian, A.H., Li, H.Y., et al. (2015). Skp2-dependent ubiquitination and activation of LKB1 is essential for cancer cell survival under energy stress. Mol. Cell *57*, 1022–1033.

Lin, H.K., Chen, Z., Wang, G., Nardella, C., Lee, S.W., Chan, C.H., Yang, W.L., Wang, J., Egia, A., Nakayama, K.I., et al. (2010). Skp2 targeting suppresses tumorigenesis by Arf-p53-independent cellular senescence. Nature *464*, 374–379.

Lin, H.K., Wang, G., Chen, Z., Teruya-Feldstein, J., Liu, Y., Chan, C.H., Yang, W.L., Erdjument-Bromage, H., Nakayama, K.I., Nimer, S., et al. (2009). Phosphorylation-dependent regulation of cytosolic localization and oncogenic function of Skp2 by Akt/PKB. Nat. Cell Biol. *11*, 420–432.

McPherson, J.P., Tamblyn, L., Elia, A., Migon, E., Shehabeldin, A., Matysiak-Zablocki, E., Lemmers, B., Salmena, L., Hakem, A., Fish, J., et al. (2004). Lats2/Kpm is required for embryonic development, proliferation control and genomic integrity. EMBO J. *23*, 3677–3688.

Nakayama, K., Nagahama, H., Minamishima, Y.A., Matsumoto, M., Nakamichi, I., Kitagawa, K., Shirane, M., Tsunematsu, R., Tsukiyama, T., Ishida, N., et al. (2000). Targeted disruption of Skp2 results in accumulation of cyclin E and p27(Kip1), polyploidy and centrosome overduplication. EMBO J. *19*, 2069–2081.

Nakayama, K., Nagahama, H., Minamishima, Y.A., Miyake, S., Ishida, N., Hatakeyama, S., Kitagawa, M., Iemura, S., Natsume, T., and Nakayama, K.I. (2004). Skp2-mediated degradation of p27 regulates progression into mitosis. Dev. Cell *6*, 661–672.

Oh, H.J., Kim, M.J., Song, S.J., Kim, T., Lee, D., Kwon, S.H., Choi, E.J., and Lim, D.S. (2010). MST1 limits the kinase activity of aurora B to promote stable kinetochore-microtubule attachment. Curr. Biol. *20*, 416–422.

Ono, H., Shimano, H., Katagiri, H., Yahagi, N., Sakoda, H., Onishi, Y., Anai, M., Ogihara, T., Fujishiro, M., Viana, A.Y., et al. (2003). Hepatic Akt activation induces marked hypoglycemia, hepatomegaly, and hypertriglyceridemia with sterol regulatory element binding protein involvement. Diabetes *52*, 2905–2913.

Pan, D. (2010). The hippo signaling pathway in development and cancer. Dev. Cell *19*, 491–505.

Pandit, S.K., Westendorp, B., and de Bruin, A. (2013). Physiological significance of polyploidization in mammalian cells. Trends Cell Biol. *23*, 556–566.

Pandit, S.K., Westendorp, B., Nantasanti, S., van Liere, E., Tooten, P.C., Cornelissen, P.W., Toussaint, M.J., Lamers, W.H., and de Bruin, A. (2012). E2F8 is essential for polyploidization in mammalian cells. Nat. Cell Biol. *14*, 1181–1191.

Serres, M.P., Kossatz, U., Chi, Y., Roberts, J.M., Malek, N.P., and Besson, A. (2012). p27(Kip1) controls cytokinesis via the regulation of citron kinase activation. J. Clin. Invest. *122*, 844–858.

Tran, H., Brunet, A., Griffith, E.C., and Greenberg, M.E. (2003). The many forks in FOXO's road. Science's STKE *2003*, RE5.

Tumaneng, K., Schlegelmilch, K., Russell, R.C., Yimlamai, D., Basnet, H., Mahadevan, N., Fitamant, J., Bardeesy, N., Camargo, F.D., and Guan, K.L. (2012). YAP mediates crosstalk between the Hippo and PI(3)K-TOR pathways by suppressing PTEN via miR-29. Nat. Cell Biol. *14*, 1322–1329.

Wang, H., Bauzon, F., Ji, P., Xu, X., Sun, D., Locker, J., Sellers, R.S., Nakayama, K., Nakayama, K.I., Cobrinik, D., and Zhu, L. (2010). Skp2 is required for survival of aberrantly proliferating Rb1-deficient cells and for tumorigenesis in Rb1+/– mice. Nat. Genet. *42*, 83–88.

Yang, S., Zhang, L., Liu, M., Chong, R., Ding, S.J., Chen, Y., and Dong, J. (2013). CDK1 phosphorylation of YAP promotes mitotic defects and cell motility and is essential for neoplastic transformation. Cancer Res. *73*, 6722–6733.

Yang, S., Zhang, L., Chen, X., Chen, Y., and Dong, J. (2015). Oncoprotein YAP regulates the spindle checkpoint activation in a mitotic phosphorylation-dependent manner through up-regulation of BubR1. J. Biol. Chem. *290*, 6191–6202.

Yu, F.X., Zhao, B., Panupinthu, N., Jewell, J.L., Lian, I., Wang, L.H., Zhao, J., Yuan, H., Tumaneng, K., Li, H., et al. (2012). Regulation of the Hippo-YAP pathway by G-protein-coupled receptor signaling. Cell *150*, 780–791.

Yu, F.X., Zhao, B., and Guan, K.L. (2015). Hippo pathway in organ size control, tissue homeostasis, and cancer. Cell *163*, 811–828.

Zhao, H., Bauzon, F., Fu, H., Lu, Z., Cui, J., Nakayama, K., Nakayama, K.I., Locker, J., and Zhu, L. (2013). Skp2 deletion unmasks a p27 safeguard that blocks tumorigenesis in the absence of pRb and p53 tumor suppressors. Cancer Cell *24*, 645–659.

Zhou, D., Conrad, C., Xia, F., Park, J.S., Payer, B., Yin, Y., Lauwers, G.Y., Thasler, W., Lee, J.T., Avruch, J., and Bardeesy, N. (2009). Mst1 and Mst2 maintain hepatocyte quiescence and suppress hepatocellular carcinoma development through inactivation of the Yap1 oncogene. Cancer Cell *16*, 425–438.

STAR★METHODS

KEY RESOURCES TABLE

REAGENT or RESOURCE	SOURCE	IDENTIFIER
Antibodies		
β-catenin [15B8] (mouse)	Abcam	Cat#ab6301; RRID:AB_305406
Yap (rabbit)	Cell signaling	Cat#4912S; RRID: AB_10694682
Phosphor-Yap(S127) (rabbit)	Cell signaling	Cat#4911; RRID: AB_2218913
P53[1C12] (mouse)	Cell signaling	Cat#2524; RRID: AB_331743
Mst1 (rabbit)	Cell signaling	Cat#3682; RRID: AB_2144632
Mst2 (rabbit)	Cell signaling	Cat#3952; RRID: AB_2196471
GAPDH[D16H11] (rabbit)	Cell signaling	Cat#5174; RRID: AB_10622025
P27 Kip1 (rabbit)	Cell signaling	Cat#2552; RRID: AB_2077837
Lats1[C66B5] (rabbit)	Cell signaling	Cat#3477; RRID: AB_2133513
Lats2 (rabbit)	Abcam	Cat#ab84158; RRID: AB_1860769
Phospho-Histone H3(Ser10)[D2C8](rabbit)	Cell signaling	Cat#3642; RRID: AB_10694226
Brdu [BU-1] (mouse)	Thermo Fisher	Cat#MA3-071; RRID: AB_10986341
Skp2[H-435] (rabbit)	Santa Cruz	Cat#sc-7164; RRID: AB_2187650
α-Tubulin[11H10] (rabbit)	Cell signaling	Cat#2125
PARP[46D11] (rabbit)	Cell signaling	Cat#9532S; RRID: AB_10695538
Acetyl-Lysine[4G12] (mouse)	Millipore	Cat#05-–515; RRID: AB_309775
Skp2[L70] (rabbit)	Cell signaling	Cat#4313; RRID: AB_2187641
P300 (rabbit)	Abcam	Cat#ab10485; RRID: AB_297224
Phospho-AKT substrate[110B7E] (rabbit)	Cell signaling	Cat#9614S; RRID: AB_331810
AKT (rabbit)	Cell signaling	Cat#9272; RRID: AB_329827
Phosphor-Akt(Ser473) (rabbit)	Cell signaling	Cat#9271; RRID: AB_329825
Foxo1[C29H4] (rabbit)	Cell signaling	Cat#2880; RRID: AB_2106495
Foxo3a[D19A7] (rabbit)	Cell signaling	Cat#9467; RRID: AB_2106672
Phosphor-Foxo1(Ser256) (rabbit)	Cell signaling	Cat#9461; RRID: AB_329831
Phosphor-Foxo1(T24)/Foxo31(T32) (rabbit)	Cell signaling	Cat#9464; RRID: AB_329842
CDK2[78B2] (rabbit)	Cell signaling	Cat#2536; RRID: AB_2276129
CDK4[DCS156] (mouse)	Cell signaling	Cat#2906; RRID: AB_2078399
CDK6[DCS83] (mouse)	Cell signaling	Cat#3136; RRID: AB_2229289
P21[12D1] (rabbit)	Cell signaling	Cat#2947S; RRID: AB_823586
Cyclin A1 (mouse)	Cell signaling	Cat#4656; RRID: AB_2071958
Cyclin D1[DCS6] (mouse)	Cell signaling	Cat#2926; RRID: AB_2070400
Cyclin E1[HE12] (mouse)	Cell signaling	Cat#4129P; RRID: AB_10831844
HA-Tag[C29F4] (rabbit)	Cell signaling	Cat#3724; RRID: AB_1549585
Flag-Tag (mouse)	Sigma-Aldrich	Cat#F1804; RRID: AB_262044
Skp2 (rabbit)	Proteintech Group	Cat#15010-1-AP; RRID: AB_2187647
γ-tubulin (mouse)	Abcam	Cat#ab11316; RRID: AB_297920
Centrin1 (rabbit)	Abcam	Cat#ab11257; RRID: AB_2244666
γ-tubulin (rabbit)	Proteintech Group	Cat#15176-1-AP;
Biological Samples		
HLiv-HCC180Sur-05 for HCC	Shanghai Outdo Biotech	http://www.superchip.com.cn
Human liver samples	Zhongshan Hospital of Xiamen University	N/A

(*Continued on next page*)

Continued

REAGENT or RESOURCE	SOURCE	IDENTIFIER
Chemicals, Peptides, and Recombinant Proteins		
DMEM	Invitrogen	Cat#41966052
Williams' Medium E	Invitrogen	Cat#32551087
Fetal Bovine Serum (heat-inactivated)	Sigma	Cat#F-9665
Insulin	Sigma	Cat#I-1882
Trypsin	Gibco	Cat#15400054
Lipofectamine 2000	Invitrogen	Cat#11668019
MK-2206 (AKT inhibitor)	Selleck Chemicals	Cat#S1078
Experimental Models: Cell Lines		
293T	ATCC	N/A
HepG2	ATCC	N/A
Experimental Models: Organisms/Strains		
Mouse:*Mst1*$^{fl/fl}$	From R. L. Johnson, University of Texas, M.D. Anderson Cancer Center, Houston, USA	N/A
Mouse:*Sav1*$^{fl/fl}$	From R. L. Johnson, University of Texas, M.D. Anderson Cancer Center, Houston, USA	N/A
Mouse:*Lats1*$^{fl/fl}$	From R. L. Johnson, University of Texas, M.D. Anderson Cancer Center, Houston, USA	N/A
Mouse:*Lats2*$^{fl/fl}$	From R. L. Johnson, University of Texas, M.D. Anderson Cancer Center, Houston, USA	N/A
Mouse: *Yap1*$^{fl/fl}$	From R. L. Johnson, University of Texas, M.D. Anderson Cancer Center, Houston, USA	N/A
Mouse: *Mst2*$^{fl/fl}$	Zhou et al., 2009	
Mouse: *Yap1*^{S127A} transgenic	Camargo et al., 2007	N/A
Mouse: *Skp2* KO	Nakayama et al., 2000	N/A
Mouse: Tg(*Alb*-Cre)21Mgn/J	Jackson Laboratory	JAX:003574
Mouse: *Trp53*$^{lox/lox}$	Jackson Laboratory	JAX:008462
Mouse: B6.129P2-*Akt1*^{tm1Mbb}/J	Jackson Laboratory	JAX:004912
Mouse: 129-*Cdkn1b*^{tm1Mlf}/J (p27 KO)	Jackson Laboratory	JAX: 003122
Oligonucleotides		
shRNA targeting sequence:*SKP2*: GGGCCAACA GAACAGAAGA	This paper	N/A
shRNA targeting sequence:p27: GAAGCGACCTGCTGCAGAA	This paper	N/A
h. *SKP2*plasmidForward primer : AAAAGGTACCATGCACAGGAAGCACCTC	This paper	N/A
h. *SKP2*plasmid Reverse primer : AAAAAAGCTTTTATTGTTTTAAAACAAGT	This paper	N/A
h. *P27*plasmid Forward primer : AAAAGGTACCATGTCAAACGTGCGAGTG	This paper	N/A
h. *P27*plasmid Reverse primer : AAAAAAGCTTTTACGTTTGA CGTCTTCTG	This paper	N/A
h. *FOXO1*plasmidForward primer : AAAAGTCGACGGATGGCCGAGGCGCCTCAG	This paper	N/A
h. *FOXO1*plasmidReverse primer : AAAAGGTACCTCAGCCTGACACCCAGCT	This paper	N/A

(*Continued on next page*)

Continued

REAGENT or RESOURCE	SOURCE	IDENTIFIER
h. *FOXO1* (S256A) plasmid Forward primer : AGGAGAAGAGCTGCAGCCATGGACAACAACAGT	This paper	N/A
h. *FOXO1* (S256A) plasmid Reverse primer : ACTGTTGTTGTCCATGGCTGCAGCTCTTCTCCT	This paper	N/A
h. *SKP2* (K68/71L) plasmid Forward primer : AGAGCCCCCCACGGTTACGGCTGTTAAGC AAAGGGAGT	This paper	N/A
h. *SKP2* (K68/71L) plasmid Reverse primer : GTCACTCCCTTTGCTTAACAGCCGTAACCGT GGGGGGCTC	This paper	N/A
h. pad.Flag. *SKP2* (KLKL) plasmid Forward primer : AAAAGGTACCGCCACCATGCACAGGAAGCACCTC	This paper	N/A
h. pad.Flag. *SKP2* (KLKL) plasmid Reverse primer : AAAAAAGCTTTTAGCCTTGTCATCGTCGTCCTTG TAGTCTTGTTTTAAAACAAGTCTA	This paper	N/A
h. pad.Flag. *FOXO1*(S256A) plasmid Forward primer : AAAAGGTACCGCCACCATGGCCGAGGCGCCTCAG	This paper	N/A
h. pad.Flag. *FOXO1* (S256A) plasmid Reverse primer : AAAAGTCGACTCATTGTCATCATCGTCCTTATAGTCG CCTGACACC CAGCTATG	This paper	N/A
m. *Sod2*qPCR Forward primer : TTAACGCGCAGATCATGCA	This paper	N/A
m. *Sod2*qPCR Reverse primer : GGTGGCGTTGAGATTGTTCA	This paper	N/A
m. *Catslase* qPCR Forward primer : TGAGAAGCCTAAGAACGCAAT	This paper	N/A
m. *Catslase* qPCR Reverse primer : CCCTTCGCAGCCATGTG	This paper	N/A
m. *G6pase* qPCR Forward primer : TGGTAGCCCTGTCTTTCTTTG	This paper	N/A
m. *G6pase* qPCR Reverse primer : TTCCAGCATTCACACTTTCCT	This paper	N/A
m. *Pepck* qPCR Forward primer : ACACACACACATGCTCACAC	This paper	N/A
m. *Pepck* qPCR Reverse primer : ATCACCGCATAGTCTCTGAA	This paper	N/A
m. *Ang2* qPCR Forward primer : GCTTCGGGAGCCCTCTGGGA	This paper	N/A
m. *Ang2*qPCR Reverse primer : CAGCGAATGCGCCTCGTTGC	This paper	N/A
m. *Fasl* qPCR Forward primer : GGCTCTGGTTGGAATGGGATT	This paper	N/A
m. *Fasl* qPCR Reverse primer : TTGGTTGGTGAACTCACGGAG	This paper	N/A
m. *Bnip3*qPCR Forward primer : AGAACCTGCAGGGCTCCTGG	This paper	N/A
m. *Bnip3*qPCR Reverse primer : GAAGTTGTCAGACGCCTTCC	This paper	N/A
m. *Ccng2*qPCR Forward primer : AGGGGTTCAGCTTTTCGGATT	This paper	N/A
m. *Ccng2*qPCR Reverse primer : AGTGTTATCATTCTCCGGGGTAG	This paper	N/A
m. *Igfbp1*qPCR Forward primer : ATCTGCCAAACTGCAACAAG	This paper	N/A

(*Continued on next page*)

Continued		
REAGENT or RESOURCE	SOURCE	IDENTIFIER
m. *Igfbp1*qPCR Reverse primer : GACCCAGGGATTTTCTTTC	This paper	N/A
m. *P27*qPCR Forward primer : TCAAACGTGAGAGTGTCTAACG	This paper	N/A
m. *P27*qPCR Reverse primer : CCGGGCCGAAGAGATTTCTG	This paper	N/A
m. *Gapdh* qPCR Forward primer : AGGTCGGTGTGAACGGATTTG	This paper	N/A
m. *Gapdh* qPCR Reverse primer : TGTAGACCATGTAGTTGAGGTCA	This paper	N/A
Recombinant DNA		
Plasmid: pCMV-Yap-mCherry	This paper	N/A
Plasmid: pCMV-Flag-p27	This paper	N/A
Plasmid: pCMV-HA-Skp2	This paper	N/A
Plasmid: pCMV-HA-Skp2(KLKL)	This paper	N/A
Plasmid: pCMV-Flag-Foxo1	This paper	N/A
Plasmid: pCMV-HA-Yap	This paper	N/A
Plasmid: pAdeasy-Myr-Flag-AKT1	This paper	N/A
Plasmid: pAdeasy-HA-Skp2	This paper	N/A
Plasmid: pAdeasy-HA-Skp2(KLKL)	This paper	N/A
Plasmid: pAdeasy-Flag-Foxo1(S256A)	This paper	N/A
Plasmid: pAdeasy-Shp27	This paper	N/A
Plasmid: pAdeasy-shskp2	This paper	N/A
Plasmid: pscAAV-GFP-shp27	This paper	N/A
Software and Algorithms		
FlowJo	https://www.flowjo.com	N/A
Prism5	GraphPad	www.graphpad.com/scientific-software/prism
R version 3.1.2	https://www.r-project.org	N/A
ImageJ	https://imagej.nih.gov/ij	N/A

CONTACT FOR REAGENT AND RESOURCE SHARING

Further information and requests for reagents may be directed to, and will be fulfilled by the corresponding author Dr. Dawang Zhou (dwzhou@xmu.edu.cn).

EXPERIMENTAL MODEL AND SUBJECT DETAILS

Mice

The mice*Mst1*$^{fl/fl}$,*Sav1*$^{fl/fl}$, *Lats1*$^{fl/fl}$, *Lats2*$^{fl/fl}$and*Yap1*$^{fl/fl}$ (from R. L. Johnson), *Mst2*$^{fl/fl}$(Zhou et al., 2009),*Skp2* KO (Nakayama et al., 2000)and *Yap1*^{S127A} transgenic mice(Camargo et al., 2007)were obtained as indicated.Wild-type C57BL/6, Tg(*Alb*-Cre)21Mgn/J, *Trp53*$^{lox/lox}$, B6.129P2-*Akt1*^{tm1Mbb}/J and 129-*Cdkn1b*^{tm1Mlf}/J (p27 KO) mice were originally purchased from the Jackson Laboratory.See "Key Resources Table" for details. All mice were maintained under specific pathogen-free conditions at the Xiamen University Laboratory Animal Center. These mouse experiments were approved by the Institutional Animal Care and Use Committee and were in strict accordance with good animal practice as defined by the Xiamen University Laboratory Animal Center.

Cell Lines and Cell Culturing

The 293T and HepG2 cell lines (from the American Type Culture Collection) were tested for mycoplasma contamination and were found to be negative, then were cultured in DMEM (invitrogen, Carlsbad, CA, USA)supplemented with 10% FBS and 1 x penicillin-streptomycin. Mouse primary hepatocytes were isolated by the two-step liver perfusion method as above described. The cells were plated in 24-well gelatin-coated plates (8 x 10^4) in Williams' Medium E (Invitrogen) containing 10% fetal bovine serum, 100 U/mlpenicillin /streptomycin and 1 × 10^{-7} M insulin, and cultured at 37 °C with 5% CO_2.

Human Liver and HCC Samples

Human samples for Western blot analysis were obtained with informed consent from human tissue banks of Zhongshan Hospital of Xiamen University. Regarding correlation analysis, we took binary logarithm ratio of the proteins expression in the cancer tissue and the matched paracancerous tissue. Since the distribution of log-ratio do not follow Gaussian distribution, we used "Spearman rank correlation coefficient" to evaluate the correlation of the log-ratios of paired proteins among p-Yap, p-Akt, Ace-skp2, FoxO1 and FoxO3a. Then the significance of correlation coefficients was tested against the null hypothesis of zero-correlation, using two-sided t-test. We adjusted the pvalue using "Benjamin & Hochberg "method and set 0.05 to the significance level. The tools for correlation analysis are available from R version 3.1.2, which can be downloaded from https://www.r-project.org. Paired cancer and adjacent non-cancer paraffin tissue sections (HLiv-HCC180Sur-05 for HCC) were purchased from Shanghai Outdo Biotech (Shanghai, China). The immunoreactive score (IRS) gives a range of 0–12 as a product of multiplication between positive cells proportion score (0–4) and staining intensity score (0–3). The IRS, 0-1, negative; 2-3, mild; 4-8, moderate; 9-12, strongly positive (Fedchenko and Reifenrath, 2014). All experiments were performed with the approval of the Xiamen University Review Board. Snap-frozen biopsies from specimens of normal liver tissue (distant from the tumor) and HCC were collected. The diagnosis of HCC or normal liver was confirmed based on histological findings by independent pathologists.

METHOD DETAILS

Hepatocyte Isolation and Ploidy Measurement

Mouse primary hepatocytes were isolated by the two-step liver perfusion method and cell ploidy was analyzed by flow cytometry. Briefly, the mouse was anesthetized with intraperitoneal injection of xylazine (10 mg/kg body weight) and ketamine (100 mg/kg body weight). The abdomen was then cut open, and the portal vein was catheterized. The liver was first perfused in situ with D-Hank's buffered solution (containing 0.5 mM EGTA, pre-warmed to 37°C) for 8-10 min with the inferior vena cava cut for drainage and then perfused for 5 min with 0.12 PZ-U/ml collagenase perfusate (containing 2 mM Ca^{2+}). The livers were extirpated and transferred into plates filled with DMEM at 4°C. The hepatic capsules were torn, and the livers were gently shaken to help the cells detach. The cell suspension was collected and filtered through 70 μm cell strainers (BD Falcon, Bedford, USA), resuspended in Percoll/DMEM/PBS (1:1:0.3) mixture and centrifuged at 50g for 15 min at RT. Cell viability was examined by the Trypan blue exclusion test (generally >90%). Purified hepatocytes were then washed with PBS and fixed with 70% ice-cold ethanol overnight. Cells were then washed with 5ml PBS and resuspended in 0.5ml of 0.25mg/ml RNase A and 10ug/ml propidum iodide in PBS for fluorescence-activated cell sorting (FACS) analysis using flow cytometer BD LSRortessa (BD biosciences). Flow cytometry data were analyzed using FlowJo software (Treestar, Ashland, USA). The polyploidy profile were quantified and plotted from three mice per genotype.

Correlation Analysis of Cell Size, Nucleus Size and DNA Content

The correlation of cell size, nuclear size and ploidy was assessed by immunefluorescence staining and FACS approaches. Hepatocytes in liver sections were labeled with DAPI (recognition of nucleus, blue) and antibody against β-catenin (a marker usually used to outline cell membrane, green, and 1:100 dilution, Abcam, ab6301). The areas of cell (cell size) and DAPI positive compartment (nucleus) were imaged with Zeiss LSM 780 and quantified by ImageJ software. In addition, the intensity value of forward-scattered light (FSC) of FACS is proportional to cell size and the intensity value of Hoechst 33342 dye staining is used to measure DNA content. Flow cytometry data were analyzed using FlowJo software (Treestar, Ashland, USA).

MEF Preparation and Infection

Embryos from timed pregnancies were harvested between E12.5-E14.5. Heads, livers, and blood clots were removed and the rest of tissues were minced and put into 1ml Trypsin (Gibco, CA, USA) for 10 min at 37°C. The tissue and Trypsin mixture was pipetted up and down several times and the dissociated cells were cultured in DMEM (invitrogen, Carlsbad, CA, USA) containing 10% fetal bovine serum (FBS) and 1 × penicillin/streptomycin. Cells were split every 3-4 days during early passages, and MEFs at passage 2 or 3 were used for infection. Parallel infection with adeno-Cre or adeno-GFP were used to delete *Lats1* and *Lats2* or *Yap* in MEFs containing floxed*Lats1/2* or *Yap*.

Hydrodynamic Gene Delivery

Hydrodynamic delivery of 100μg of pCMV-Yap-mCherry or control mCherry plasmid in 2 ml of Ringer's solutions (147 mMNaCl, 4 mMKCl, 1.13 mM CaCl2) were done via tail vein injections within 5 s.

Generation of Recombinant Adenovirus

Recombinant adenovirus was generated using standard techniques. Briefly, the myr-Akt1, Skp2 (WT), Skp2(KLKL) and FoxO1 (S256A) cDNA were subcloned into the multicloning site of the AdTrack-CMV shuttle vector, which contains a GFP as a reporter gene. The Myr-Akt1, Skp2 (WT) and Skp2 (KLKL) cDNA were inserted between the KpnI–XhoI restriction sites; FoxO1(S256A) cDNA was inserted between the KpnI–SalI restriction sites. The shRNA against p27 (Shp27) oligo pairs were annealed and subcloned into the polylinker region of the pLL3.7 vector and then cut by XhoI and XbaI restriction enzyme. The fragment containing Shp27 was subcolned into the polylinker region between the cytomegalovirus promoter and polyadenylation sequences the AdTrack shuttle

vector, which contains a GFP as a reporter gene. The resultant plasmid was linearized by digestion with PmeI endonuclease and cotransformed into *Escherichia coli* BJ5183 cells with the AdEasy-1 adenoviral plasmid, which contains the entire genomic sequences of adenovirus serotype Ad5, except the nucleotides encompassing the E1 and E3 genes. Recombinant bacteria were selected by kanamycin resistance and the recombination was confirmed by a PacI endonuclease restriction analysis. The Ad-GFP was constructed similarly. Subsequently, the verified clone was amplified, linearized with PacI and transfected into HEK293A packaging cells. The recombinant adenovirus was released from the cells by four freeze–thaw–vortex cycles 14–20 days post transfection, amplified by further rounds of infection of HEK293A packaging cells and purified by CsCl ultracentrifugation. Stocks of purified adenovirus were titred by counting the number of plaque-forming units. The recombinant adenoviruses (2×10^9pfu in 200 ml PBS) were injected into 6- to 8-week-old male mice via the tail vein.

shRNA and Lentiviral Infection

The shRNA-targeted sequencesagainst p27 and Skp2 were synthesized. Oligo pairs were annealed and subcloned into the polylinker region of the pLL3.7 vector. Lentivirus was produced by co-transfecting 293T cells with the shRNA in the vector pLL3.7, VSV-G and Δ8.9 plasmids using Lipofectamine 2000 (Invitrogen). Viral supernatant was harvested at 48-72 h post-transfection, passed through a 0.45 μm filter, diluted 2:3 with fresh medium containing 8 μg/ml polybrene and used to infect the target cells at 80% confluence. Protein expression was visualized by immunoblotting.

Generation of AAV-Shp27 Virus

The shRNA-targeted p27 sequence and scramble control sequence were synthesized. Oligo pairs were annealed and subcloned into the pscAAV-GFP vector (Addgene#32396). 293 T cells were co-transfected with scAAV shRNA or control plasmid, adenovirus helper plasmid PXX6 and AAV8 helper plasmid p5E18-VD28. Cells were harvested 60 hr post transfection. The crude virus were released from 293T cells after 3 times of freezing and thaw, and then further purified with chloroform treatment and PEG8000-(NH4)2SO4 partition. The virus fraction were dialyzed in PBS solution and concentrated by Amicon Ultra centrifugal filter. The AAV titer was determined by RT-PCR using primers against the CMV promoter on the AAV vector. Mice were infected with AAV virus at $1x10^{11}$ virus copies per mouse via tail vein injection.

Real-Time Quantitative PCR

One microgram of total RNA from the liver tissue or cells was reverse transcribed with oligo dT and Superscript III reverse transcriptase (Invitrogen). Real-time quantitative PCR was performed using a BioRadiQ SYBR Green Supermix kit and the BioRadiCycleriQ system (BioRad, Hercules, CA, USA). All runs were accompanied by the internal control *Gapdh* gene. The samples were run in triplicate and normalized to Gapdh using a ΔΔ cycle threshold-based algorithm, to provide arbitrary units representing relative expression levels. Each graph is representative of at least three independent experiments.

SDS-PAGE and Immunoblot Analysis

Proteins were separated by SDS-PAGE, were transferred onto a PVDF membrane and then were identified by immunoblot analysis with the appropriate primary antibodies at a dilution of 1:1,000. Horseradish peroxidase–conjugated antibody to rabbit IgG (7074) or to mouse IgG (7076) (1:3,000 dilution for each) were from Jackson ImmunoResearch Laboratories. The protein bands were visualized with a SuperSignal West Pico Kit according to the manufacturer's instructions (Thermo Fisher Scientific Pierce).

Immunofluorescence Staining

The cells were washed three times with PBS and were fixed for 15 min at room temperature with 4% (vol/vol) paraformaldehyde, after which additional immunofluorescence staining was applied. The primary antibodies,anti-HA (1:250 dilution; Santa Cruz sc-7392), anti-Flag (1:500 dilution; Sigma), anti-α-tubulin (1:250dilution; Cell signaling, 2125), anti-Skp2 (1:100 dilution; Proteintech, 15010-1-AP), anti-γ-tubulin (1:250 dilution; Abcam ab11316), anti-Centrin1 (1:250 dilution; Abcam ab11257) or anti-γ-tubulin (1:200 dilution; proteintech 15176-1-AP) were used.Fixed cells were rinsed with PBS and then were incubated for 10 min on ice with 0.2% Triton X-100 and 0.2% BSA in PBS. Following permeabilization, nonspecific binding in the cells was blocked by incubation for 30 min at room temperature with 0.02% Triton X-100 and 5% BSA in PBS and cells were incubated for 1 hr with specific primary antibodies (identified above). After three washes with PBS, the cells were incubated for another 1 hr with secondary antibodies (Alexa Fluor 488–conjugated anti–mouse IgG (A21202), Alexa Fluor 488–conjugated anti–rabbit IgG (A21206) or Alexa Fluor 555–conjugated anti–mouse IgG (A31570) (all from Invitrogen). Subsequently, the cells were washed three times with PBS and were mounted with Vectashield mounting medium containing DAPI. All images were collected with a confocal microscope (Zeiss LSM 780).

Immunohistochemistry

The tissue specimens were fixed overnight in 10% neutral-buffered formalin and then were dehydrated in increasing concentrations of isopropyl alcohol, followed by clearing of alcohol by xylene. The specimens were subsequently embedded in paraffin wax in cassettes for facilitation of tissue sectioning. Standard staining with hematoxylin and eosin was performed on sections 5 μm in thickness from each specimen block. For immunohistochemistry, liver sections were deparaffinized and incubated in citrate buffer at 95°C for 40 min for antigen retrieval and then incubated overnight at 4 °Cwith the primary antibodies including anti-BrdU (1:100 dilution, life technologies, MA3-071), anti-pHH3 (1:100 dilution, Cell signaling, 3377), anti-Yap (1:500 dilution, Cell signaling, 14074), anti-Skp2

(1:100 dilution, proteintech, 15010-1-AP), anti-p27 (1:100 dilution, Cell signaling 2552), anti-Foxo1 (1:100 dilution, Cell signaling, 2880), anti-Foxo3a (1:100 dilution, Cell signaling, 12829) and antibody to phosphorylated Akt (1:50 dilution, Cell signaling ,9271s). After three washes, tissue sections were incubated with biotinylated anti-mouse IgG (1:200 dilution, Vector Laboratories, CA, USA) for 1 hr at RT and then washed three times, after which streptavidin–horseradish peroxidase conjugates (Vector Laboratories, CA, USA) were added and the slides incubated for 45 min. After three washes with PBS, DAB solution (Vector Laboratories, CA, USA) was added and the slides were counterstained with haematoxylin.

Clonogenic Assay for the Cell-Survival Experiment

Cells were trypsinized and counted with a hemocytometer. Three milliliters of DMEM full medium containing 500 cells was plated in each of the three wells in the six-well plate. The cells were maintained at 37 °C for 7 days to allow the formation of colonies and were then stained with 0.5% crystal violet (Sigma-Aldrich) in absolute methanol.

Treatment of Mice with Akt Inhibitor MK2206

MK-2206 (obtained from Selleck Chemicals) was prepared in 30% (v/v) Captisol (CyDex Pharmaceuticals). Mice were randomized into two groups: vehicle control or MK-2206-treated. For short-term treatment, 8-week-old WT or Mst1/2 DKO mice were administered at a dose of 200 mg/kg by oral gavage three times per week for 2 weeks. For the long-term therapy, 12-week-old WT or Mst1/2 DKO mice were administered at a dose of 200 mg/kg by oral gavage three times per week for 8 weeks. The control group received vehicle only. Liver tissues used for RNA purification, protein extraction or histology were harvested at the indicated times.

QUANTIFICATION AND STATISTICAL ANALYSIS

All data are representative of at least three independent experiments. All statistical analyses were performed using Prism5 (GraphPad). The data are presented as the mean± SD and Student's t test was used for comparisons between two groups. Survival data was analyzed using Kaplan–Meier statistical method. The ratio of the relative expression of the indicated proteins from the tumor patients was plotted and applied with the linear regression ttest. A p value 0.05 was considered statistically significant. In the graphed data *, **, and *** denote p values of < 0.05, 0.01 and 0.001, respectively.